DEVELOPMENT OF MATHEMATICAL MODEL FOR ESTIMATION OF CELL DENSITY IN ISOTROPIC CLOSED-CELL FOAMS USING CRITICAL BUBBLE LATTICE METHOD

PIYAPONG BUAHOM

A THESIS SUBMITTED IN PARTIAL FULFILLMENT
OF THE REQUIREMENT FOR THE DEGREE OF
MASTER OF ENGINEERING IN CHEMICAL ENGINEERING
FACULTY OF ENGINEERING
KING MONGKUT'S INSTITUTE OF TECHNOLOGY LADKRABANG
2010

หัวข้อวิทยานิพนธ์	**การพัฒนาแบบจำลองทางคณิตศาสตร์สำหรับการประมาณค่าความหนาแน่นเซลล์ของโฟมไอโซโทรปิกแบบเซลล์ปิดด้วยวิธีโครงผลึกของฟองก๊าซวิกฤต**
นักศึกษา	**นายปิยพงศ์ บัวโฮม**
รหัสนักศึกษา	51061103
ปริญญา	**วิศวกรรมศาสตรมหาบัณฑิต**
สาขาวิชา	**วิศวกรรมเคมี**
พ.ศ.	2553
อาจารย์ที่ปรึกษาวิทยานิพนธ์	**ผศ. ดร. สุรัตน์ อารีรัตน์**

บทคัดย่อ

การศึกษานี้ได้ทำการพัฒนาแบบจำลองสำหรับการประมาณค่าความหนาแน่นเซลล์ของโฟมไอโซโทรปิกพอลิเมอร์แบบเซลล์ปิดด้วยพารามิเตอร์ความหนาแน่นเซลล์บนระนาบ โดยได้พัฒนาแบบจำลองโครงผลึกของฟองก๊าซวิกฤตสำหรับเชื่อมโยงโครงสร้างการจัดเรียงตัวของอะตอมแบบ Face-Centered Cubic (FCC) กับโครงสร้างเซลล์ของโฟมพอลิเมอร์แบบเซลล์ปิดซึ่งโดยทั่วไปมีรูปร่างเซลล์เป็นทรงสิบสองหน้า เพื่อประยุกต์ใช้วิธีการประมาณค่าความหนาแน่นอะตอมมาใช้หาความหนาแน่นเซลล์ของโฟม โดยได้พัฒนาแบบจำลองเพื่อศึกษาผลของความไม่เป็นอุดมคติของหน้าตัดเซลล์ที่ปรากฏบนไมโครกราฟ 2 กรณี คือ แบบจำลองหน้าตัดเซลล์แบบอุดมคติ (FCC-PF) และแบบจำลองหน้าตัดเซลล์แบบไม่อุดมคติ (FCC-NPF) พบว่าความสัมพันธ์ระหว่างความหนาแน่นเซลล์กับความหนาแน่นเซลล์บนระนาบแสดงให้เห็นถึงผลของความไม่เป็นอุดมคติของหน้าตัดเซลล์ที่ปรากฏบนไมโครกราฟ ซึ่งความหนาแน่นเซลล์มีค่าอยู่ระหว่างแบบจำลองที่พัฒนาขึ้นทั้งสอง โดยแบบจำลองหน้าตัดเซลล์แบบไม่อุดมคติมีความเหมาะสมในการประมาณค่าความหนาแน่นเซลล์ของโฟมความหนาแน่นต่ำโดยมีค่าความเบี่ยงเบนสัมบูรณ์เฉลี่ยร้อยละ 53.2 ส่วนแบบจำลองหน้าตัดเซลล์แบบอุดมคติมีความเหมาะสมในการประมาณค่าความหนาแน่นเซลล์ของโฟมความหนาแน่นสูงโดยมีค่าความเบี่ยงเบนสัมบูรณ์เฉลี่ยร้อยละ 68.8 ซึ่งแบบจำลองทั้งสองที่พัฒนาขึ้นมีความน่าเชื่อถือในการประมาณค่าความหนาแน่นเซลล์มากกว่าสมการเฉลี่ยอย่างง่ายที่ใช้กับโฟมทั่วไปที่มีค่าความเบี่ยงเบนสัมบูรณ์เฉลี่ยร้อยละ 405.9 สำหรับโฟมความหนาแน่นต่ำและร้อยละ 72.0 สำหรับโฟมความหนาแน่นสูง นอกจากนี้ยังได้พัฒนาวิธีการวิเคราะห์ความเป็นไอโซโทรปิกของโฟมพอลิเมอร์ด้วยดัชนีไอโซโทรปิกโฟม (Isotropic foam index) ซึ่งค่าดัชนีไอโซโทรปิกโฟมของโฟมไอโซโทรปิกพอลิเมอร์ความหนาแน่นต่ำแบบเซลล์ปิดมีค่าอยู่ในช่วง 0 ถึง 0.895

Thesis Title	Development of Mathematical Model for Estimation of Cell Density in Isotropic Closed-Cell Foams using Critical Bubble Lattice Method
Student	Mr. Piyapong Buahom
Student ID.	51061103
Degree	Master of Engineering
Program	Chemical Engineering
Year	2010
Thesis Advisor	Asst. Prof. Dr. Surat Arerat

Abstract

In this study, models for estimating the cell density of isotropic polymeric closed-cell foams using the surface cell density were developed. The basic morphological unit cell for these models is a gas-filled pentagonal dodecahedral cell cavity. The critical bubble lattice model was introduced to associate the packing structure of the pentagonal dodecahedron cells with a face-centered cubic (FCC) packing structure, and the cell density was estimated. This model was then used to investigate the effect of non-perfect cell cross-sections as found in the micrographs of cell densities of foams. Two cases were examined: first, the ideal case of a perfect cross-section (FCC-PF), and second, the actual experimental case of a non-perfect cross-section (FCC-NPF). The plot of cell density versus surface cell density from recently published data show the effect of a non-perfect cross-section on the estimation of cell density within an FCC lattice with perfect and non-perfect cell cross-sections. The percentage average absolute deviation (AAD) showed that the non-perfect cell cross-section model reliably predicts the cell density of isotropic low density foam with an AAD of 53.2%. The perfect cell cross-section model reliably predicts the cell density of isotropic high density foam with an AAD of 68.8%. These new models are more reliable than the conventional model, which gives AADs 405.9% for low density foams and 72.0% for high density foams. Furthermore, the isotropic foam index was introduced as a parameter to indicate the isotropic foam behavior. The isotropic foam index of isotropic low density foams is within the range of 0 and 0.895.

Acknowledgements

This thesis could not be complete without the assistance of many persons to whom I would like to express my appreciation.

First, I would like to express my deepest gratitude to my research advisor Assistant Professor Dr. Surat Areerat, who has given me many helpful suggestions, useful advice, fruitful discussions during the undertaken research and constant support in helping me to conduct and complete this work.

I would like to thank Thai Polyethylene Co. Ltd. for polyethylene blends. I would also like to thank Mr. Ratchaphon Tangnopadol and Dr. Wuttipong Rungseesantivanon from National Metal and Materials Technology Center (MTEC) for providing sisal fiber-reinforced polypropylene composite. Moreover, I would like to acknowledge Professor Masahiro Oshima and Assistant Professor Kentaro Taki in the Chemical Engineering Department at Kyoto University for their helpful suggestions, as well as for their generous advice.

Special thanks go to my friends at School of Chemical Engineering for their kindness and help provided during my studies at KMITL.

Finally, I want to extend my profound appreciation to my family and relatives for their love, affection, understanding, motivation, and invaluable support during my life and studies.

Piyapong Buahom

Contents

Contents (cont.)

Contents (cont.)

Contents (cont.)

List of Tables

List of Tables (cont.)

List of Figures

List of Figures (cont.)

List of Figures (cont.)

List of Figures (cont.)

Nomenclature

Symbols

A	Area of Interest
$\bar{A}$	Average cell cross-sectional windows area
d	Bubble size; average diameter of bubbles
D_C	Cell size or diameter of critical bubble
N_S	Surface cell density
N_F	Cell density
N_O	Nucleus density
n	Number of cells, nuclei or bubble of interest
V	Volume

Greek Symbols

ϕ	Volumetric expansion ratio
ε	Void fraction
ρ	Bulk density
κ	Apparent factor
α	Periodic factor
φ	Isotropic factor
η	Isotropic foam index

Subscripts

bb	Unit bubble
CR	Critical bubble
G	Gas
HD	High density foams
LD	Low density foams
P	Polymer resin or unfoamed polymer
T	Total

Superscripts

*	True value
o	Standard or reference value

Chapter 1

Introduction

1.1 Context and Motivation

Polymeric foams are made up of gas that disperses in a dense continuum liquid or solid polymer. Gas bubbles nucleate and grow in the liquid polymer during production. The foam has a microstructure that randomly distributed cells of various shapes and sizes filled the space completely [1]. Polymeric foams exhibit many advantages over unfoamed polymers such as higher in toughness, impact strength, stiffness to-weight ratio, and thermal stability, while lower in density, dielectric constant and thermal conductivity [2-5]. From these reason, polymeric foams are widely used in industry and in domestic applications such as packaging materials, insulation, controlled release devices, filtration membrane, sports equipment, airplane and automotive parts [6-7]. The advantages of microcellular structures led to the development of various foaming techniques applied to such processes as batch foaming, thermoforming, continuous filament and sheet extrusion, and injection molding [8].

The physical and mechanical properties of cellular foams are governed by two parameters, i.e., bulk density and cell morphology [9]. The bulk density has been widely used as a predictor of their mechanical properties due to the simplicity of measurement with high precision methods ASTM D1622 and ISO 845 [14-15]. Cell size distribution of foam can be different in three dimensions, causing difficulty of measuring foam morphology. Cell density and cell size are main parameters in characterization of foam morphology, and affect to the cell size distribution and uniformity of the structure that associated with the foam formation process [9-11]. Recently, cell density was used as a main parameter to validate mechanical models for polymeric foams on impact properties [12-13]. Moreover, cell density was used to approximate nucleation density that refers to the number of nuclei in unit volume of unfoamed polymer, and used to describe the nucleation process of foam formation with assumption of no coalescence and no breakup of gas bubbles in bubble growth process [3, 9].

At present, the true cell densities of microcellular foams are still not well-estimated. The estimation of cell density of isotropic foam has been using wildly with conventional stereological average and material balance-based methods. The conventional stereological method is simple

and rough, the estimation is used the surface cell density that represent the population density of the foam bubbles on micrograph as a parameter, then surface cell density would be converted to 3D cell density by the assumption that bubble dispersion is uniform in all direction. While, the material balance-based model includes parameters that are more important, i.e., expansion ratio and average cell size [2, 9]. However, the material balance-based method is being currently the most reliable. Both the material balance-based and conventional models give similar results for high density polymeric foams, while the different models do not give similar results for low density isotropic foams [9]. However, in case of irregular or complex shapes of gas bubbles, the estimation by material balance-based cell density method is difficult to define the sizes of gas bubbles.

This work studied in estimation of cell density in isotropic polymeric foams. Analysis of foam microstructure including cell boundary was used to perform estimating cell density with independent of sizes and shapes of the bubbles inside the cells. Surface cell density on micrograph is a main parameter of the estimation. Similarity between cell microstructure of a foam and atomic packing structure assists to estimate the foam cell density with the cell density estimation of the atomic packing. Perfect and non-perfect cell cross-sections of pentagonal dodecahedral foams were modeled to study the range of estimation due to uncertainty cross-section that affect to surface cell density observed from micrograph. Furthermore, a new method of investigating isotropic foam behavior was introduced.

1.2 Objectives

1. To develop a mathematical model for estimation of cell density by analyzing cell structure and cell size, which independent to bubble shape, bubble size, or foam processing, for both post-production isotropic high density and isotropic low density closed-cell foams.

2. To develop a method for characterization of isotropic polymeric foams behavior.

1.3 Scopes of the Study

1. This work only attempts to address issues directly related to the estimation of cell density for isotropic polymeric foams. Attention is given to how to associate pentagonal dodecahedral cell structure of foams with face-centered cubic (FCC) atomic packing structures.

2. This work attempts to develop a mathematical model that explains effects of foam structure and cell cross-section on the estimation of cell density.

3. Effect of perfect and non-perfect cell cross-sections in estimate cell density of pentagonal dodecahedron foams was studied to investigate the possible range of estimation.

4. Appropriated models and their parameters which accorded to experimental data for isotropic high density and low density closed-cell foams will be used as the standard model for each case, and used as the defined standard isotropic parameters for standard isotropic foams.

5. The method of analysis isotropic behavior of foam only attempt to develop a parameter to indicate the deviation from standard isotropic foams. Theoretical range of deviation for low density foams was also studied.

1.4 Assumptions of the Study

1. Cell density of foam equals to cell density of similarly atomic packed structure.

2. Characterization of cell density based on cell boundary is independent to bubble size and bubble shape inside.

1.5 Limitations of Study

Limitations of study are reliability in characterizations of some parameters as follows:

1. Uncertainly measurable of true cell density.

2. Uncertainty estimation of surface cell density.

3. Non-uniform and non-isotropic cell microstructures of a foam sample.

1.6 Research Methodology

1. Identify the significant problems, objectives, scopes, and limitations of the study.

2. Study the theoretical background and literature review.

3. Develop the mathematical models for cell density estimation and isotropic foam behavior indication.

4. Model the FCC-PF and FCC-NPF models and study range of estimation.

5. Test and validate the models and investigate its parameters.

6. Investigate the standard value for isotropic high density and low density foams.

7. Test the developed method of characterization of isotropic foam properties.

8. Conclude the results and write report.

1.7 Outcomes of the Thesis

1. A mathematical model for cell density determination of isotropic closed-cell foams using surface cell density which is based on principle of material balance and foam microstructure model.

2. An analytical method for characterization of isotropic polymeric foams.

Chapter 2

Literature Review and Theoretical Background

This chapter presents a literature survey on the theoretical studies and practices on cell density determination in polymeric foams. It includes the backgrounds in polymeric foam preparation, classifications of foams, foam properties, existing methods of cell density estimation, background in atomic packing structure, and background in foam cell structural models such as foam microstructure, and cell cross-section.

2.1 Background in Polymeric Foams

This section explains some backgrounds of polymeric foams. First, the background of foam was introduced. Then, the basic concepts of cellular foaming process and classifications of polymeric foams by various criteria were described.

2.1.1 Polymeric Foams

The word "polymeric foam" refers to gas voids dispersed in a dense continuum liquid or solid polymer. Polymeric foams are three-dimensional polymeric cellular materials made from an interconnected network of the edges and faces of cells [16-17]. The idea of preparing polymeric foam with gas bubbles less than 100 μm in diameter was pioneered by Professor Nam Suh at Massachusetts Institute of Technology in the 1980s, to introduce how to reduce the amount of plastic used in mass produced items [18]. Polymeric foam is good for a wide variety of applications. Polymeric foams have been widely used because of their beneficial properties such as lightweight, thermal and acoustic insulation, and improved energy-absorption performance on impact. At present, polymeric foams were prepared by batch, extrusion, injection molding, extrusion blow molding, and thermoforming processes. The products of polymeric foaming include insulation foam boards, pipes, retail packaging, cushioning inserts, automotive and aircraft part housings, building supplies, casings for lighting, appliances, and electronics can be produced with these processes [19].

2.1.2 Cellular Foaming Process

There are four steps involved in a cellular foaming process [20-21], as shown in Figure 2.1 and explained as follows:

1) Gas Dissolution

Dissolution of gas in a polymer is to form a saturated gas/polymer solution by pressure and/or mixing into solid and liquid polymer.

2) Cell Nucleation

Cell nucleation is driven by thermodynamic instability because of an increase in temperature or a decrease in pressure, phase separation takes place between the polymer and gas to form cell nuclei. Thermodynamic instability may result from an increase in temperature and/or a decrease in pressure. If the bubbles are generated from a single homogeneous phase containing no impurity or dirt, then the process is called homogeneous nucleation. If tiny particles are present in the liquid, and if they assist in the formation of cells, then the process is called heterogeneous nucleation, since the nucleation took place at a solid and liquid interface.

3) Cell Growth

After cell nucleation, gas bubbles increase size within the polymer; the bubbles grow due to the diffusion of excess gas in the polymer. The viscosity of the polymer, the gas concentration, the foaming temperature, and the amount of nucleating agent and its nature are some of the variables that control the cell growth step.

4) Cell Stabilization

As seen in Figure 2.1, the cell growth process is stopped by a natural or an imposed ending of the driving force for cell growth. Then, cellular foam is obtained. Cooling becomes a natural way to enhance material strength to keep the foamed product stable. When foaming is completed, the polymer is cooled into a solid stable state for applications.

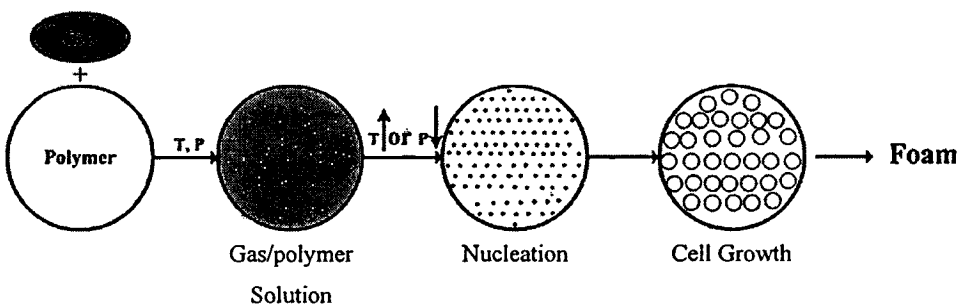

Figure 2.1 Cellular foaming process [20].

2.1.3 Classification of Polymeric Foams

Current systems of classifying types of foams depended on criteria of interest, such as foam structure, foaming process, bubble shape, size distribution, and isotropic behavior. The usually classification of foams can be done according to various methods thereof:

1) Classification Base on Foam Structure

A partition of solid foam is called a "cell". Because solid foams are derived from liquid ones, the shapes of solid foam cells and liquid foam bubbles are similar. There are two types of cell in artificial foams: closed-cell and open-cell foams [1, 18, 22] (see Figure 2.3), described as follows:

1.1) Closed cell foams has network of edges and faces still exist separately in the cells like foam bubbles, as shown in Figure 2.2A. In closed-cell foams, most cells have cell walls, the cell faces shared by the neighboring cells. Gas cannot flow through these neighbor cells.

1.2) Open cell foams comprises only the network of edges without cell faces, which only comprises a framework of struts being interconnected at the vertices of cells. Gas can flow through neighbor cells, as shown in Figure 2.2B.

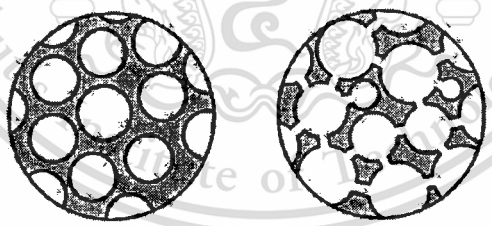

(A) (B)

Figure 2.2 Schematic of (A) closed cell foams and (B) open-cell foams [22].

2) Classification Base on Cell Geometry

Cell geometry is one of main criteria in analysis of foam morphology. The geometry of cells may be different, depended on foam formation and processing. There are mainly four types of cell geometry thereof: spherical, ellipsoidal, regular polyhedral and irregular polyhedral bubbles.

2.1) Spherical bubble, in Figure 2.3A, is a shape of ideal expansion with uniform shear stress in all direction in bubble growth step [9], such as injected foams.

2.2) Ellipsoidal bubble, in Figure 2.3B, transformed from spherical bubble due to non-uniform shear stress cause by extrusion process [9, 23].

2.3) Regular polyhedral bubble, such as hexahedron, octahedron, tetrakaidecahedron, or dodecahedron, as shown in Figure 2.4.

2.4) Irregular polyhedral bubbles, the most of real cell geometry are random, which are irregular polyhedral cells. Irregular polyhedral cells consist of irregular polygons for each side of cells, as shown in Figure 2.5.

Figure 2.3 Geometry of (A) spherical bubble and (B) ellipsoidal bubble.

Figure 2.4 Various regular polyhedral unit cells of foams: (A) regular hexagonal or simple cubic, (B) tetrakaidecahedron, (C) rhombic dodecahedron, and (D) pentagonal dodecahedron [23].

Figure 2.5 (A) Cells extracted from the random foam and (B) skeletal drawing of their cells [24].

3) Monodispersed and Multidispersed Foams

Many types of foam are non-uniform in size due to different properties of polymer bases such as melt temperature and viscosity and foam processing. There are main two types of foams in classification by cell size distribution [25] as follows:

3.1) Monodispersed foams are uniform size distribution foams are the foam which uniform in size with single peak of size normal distribution. The foam, which is single size distribution, is called mono-size structure or monomodal foam, as in Figure 2.6A.

3.2) Bimodal foam is a multidispersed with two-size distributions cellular structure, as in Figure 2.6B.

3.3) Multimodal foam is non-uniform multidispersed foam, which consist of size distribution greater than two size distributions as in Figure 2.6C.

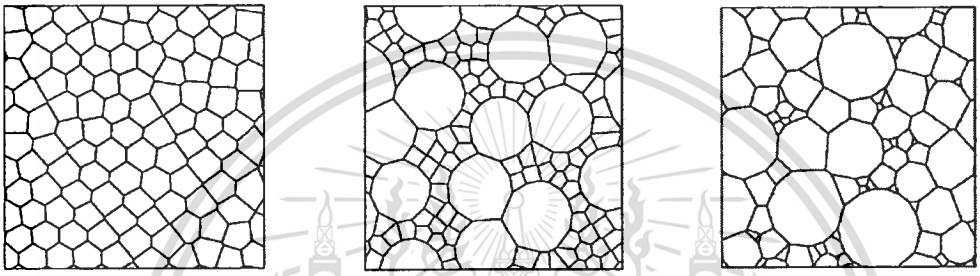

(A) (B) (C)

Figure 2.6 Four examples of microstructures generated with radical plane method: (A) mono-size cells, (B) two-size cell distribution, and (C) multimodal cell size distribution microstructure [25].

4) Classification Base on Isotropic Property

The term isotropic foam and derivatives there of means a cell whose size and structure are essentially uniform in all directions, including periodic patterned cell structures. Classification of foams by isotropic property can be collect in two groups as follows [26]:

4.1) Isotropic foams are the foam that their properties are isotropic and their cell shapes are regular.

4.2) Non-isotropic foams are the foams that their properties are not isotropic foams.

2.2 Characterizations of Foam Properties

In this section, characterizations of foam properties, i.e., bulk density, void fraction, relative density, volume expansion ratio, average bubble size, surface cell density, cell density and nucleus density, were introduced.

2.2.1 Bulk Density

Bulk density is quite easy to determine with high precision method, following the standards of ASTM D1622 and ISO 845:

(1) ASTM D1622 – Standard test method for apparent density of rigid cellular plastics is used to investigate bulk density of foams (ρ_F) [10].

(2) ISO 845 – Standard test method for cellular plastics and rubbers: is used to investigate bulk density of polymer (ρ_P). Density can be evaluated as the apparent overall density (includes forming skins) or by apparent core density (forming skins removed) [11].

2.2.2 Void Fraction

Volume expansion ratio (ε) represents the ratio of gas volume (V_G) and volume of foam (V_F), as in Equation (2.1).

$$\varepsilon = \frac{V_G}{V_F} \tag{2.1}$$

2.2.3 Relative Density

Relative density (R_F) represents the ratio between bulk density of foams (ρ_F) and bulk density of polymer (ρ_P), as in Equation (2.2).

$$R_F = \frac{\rho_F}{\rho_P} \tag{2.2}$$

2.2.4 Volume Expansion Ratio

The volume expansion ratio of the foamed (ϕ), defined as a parameter which represent the ratio of expanded volume (V_F) and unfoamed polymer (V_P), as in Equation (2.3).

$$\phi = \frac{V_F}{V_P} \tag{2.3}$$

Expansion ratio can be measured by using the ratio of bulk density of polymer and bulk density of foams, as expressed in Equation (2.4), with the assumption that mass of gas less than that of polymer relatively.

$$\phi = \frac{\rho_P}{\rho_F} \tag{2.4}$$

Equations (2.2) and (2.4) give the relationship in Equation (2.5).

$$\phi = \frac{1}{R_F} \tag{2.5}$$

In addition, the total volume of foam equals the volume of the polymer plus the volume of gas bubbles, as in Equation (2.6).

$$V_T = V_P + V_G \tag{2.6}$$

Consequently, combining Equations (2.1), (2.3) and (2.6) gives the volume expansion ratio as a function of the void fraction, as in Equation (2.7).

$$\phi = \frac{1}{1-\varepsilon} \tag{2.7}$$

2.2.5 Average Bubble Size

Average bubble size can be investigated using measured bubble diameter of each cell (d_i) and the number of each cell diameter (n_i), then calculate by Equation (2.8) [30]:

$$d = \frac{\sum(d_i n_i)}{\sum n_i} \tag{2.8}$$

2.2.6 Surface Cell Density

Surface cell density (N_S) is a morphological parameter in determination of number of cell (n) per unit area of interest (A) from micrograph, as in Equation (2.9).

$$N_S = \frac{n}{A} \tag{2.9}$$

Determination of cell density is not an exact operation because it is not possible to measure the exact surface area (A) of the area of interest (AOI) and the exact cell count (n). Two techniques for estimation of surface cell density are known AOI size and known cell count methods, as described below.

1) Known AOI size method

Known AOI size technique consists of tracing a shape of a known area, the simplest case being a rectangle and counting the circumscribed cells. The difficulty of this technique is to determine the proper number of cells to include in the cell count. As shown in Figure 2.7, There are three possible cases:

1.1) Consider only the cells strictly circumscribed in the AOI. This technique underestimates the true cell count, therefore underestimating the actual cell density, as minimum surface cell density.

1.2) Consider all the cells overlapping the AOI. This technique overestimates the true cell count, therefore overestimating the actual cell density, as maximum surface cell density.

1.3) Consider the cells strictly circumscribed in the AOI and inner part of the cells overlapping the AOI. This technique should represent more closely the actual case. Unfortunately, it is difficult to determine the fraction of border cells to consider.

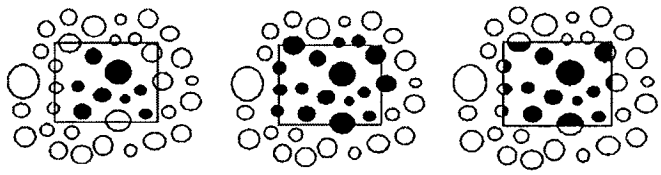

(A) (B) (C)

Figure 2.7 Known AOI size method: (A) strictly circumscribed gives minimum count (n=8), (B) complete cells gives maximum (n=17) and (C) circumscribed fraction gives mean (n=12.5) [9].

2) Known cell count method

In known cell count technique, the exact cell count is known but the exact AOI circumscribing the determined cells is uncertain. The exact value reasonably stands between two identifiable extremes, as shown in Figure 2.8. There are two possible cases:

2.1) The smallest AOI case is limited by the outer limit of the counted cells. This technique underestimates the true surface, as the maximum surface cell density.

2.2) The largest AOI case is limited by the inner limit of the adjacent surrounding cells. This technique overestimates the true surface, as the minimum surface cell density.

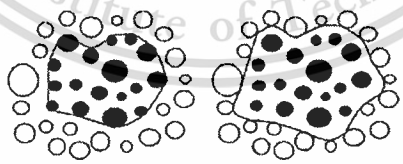

(A) (B)

Figure 2.8 Known cell count method: (A) maximum surface cell density and (B) minimum surface cell density [9].

In all cases, the maximum and minimum possible measured surface cell densities were used to determine the averaged surface cell density.

The methods of both known cell count and known AOI size to determine surface cell count give similar results within 20% uncertainty [9].

2.2.7 Cell Density and Nucleus Density

When characterizing the number of cells (n) per unit volume, there is a distinction to be made between nucleation density and cell density. Both represent a cell count but they use a different reference for the volume [2, 9]. Nucleus density (N_o) is defined as the number of nuclei (n_o) per unit volume of the original (unfoamed) polymer (V_P), as in Equation (2.10).

$$N_o = \frac{n_o}{V_P} \tag{2.10}$$

While cell density (N_F), defined as the number of cells (n_F) per unit volume of the foams (V_F) as in Equation (2.11).

$$N_F = \frac{n_F}{V_F} \tag{2.11}$$

Polymeric foams made by foaming processes usually possess a solid skin. It is possible to thermoform the polymeric foam into different shapes without collapsing the cell structure [25]. Considered that there is no coalescence and collapsed expansion in the bubble step, as shown in Figure 2.9, the numbers of nuclei and foamed cells are equal (n_O=n_F).

Figure 2.9 No coalescence and no collapsed expansion in bubble-growth step.

Combining volume expansion ratio in Equations (2.3) with nucleus density and cell density in Equations (2.10) and (2.11), lead to Equation (2.12).

$$\phi = \frac{N_o}{N_F} \tag{2.12}$$

Therefore, relationship between nucleus density and cell density can be written in conventional forms in Equations (2.13), as introduced in a work by C.B. Park [27].

$$N_o = N_F \phi \tag{2.13}$$

The relationship between expansion ratio and void fraction, in Equation (2.7), lead to the estimating cell density, which can be expressed in Equation (2.14) as introduced by K. W. Suh *et al.* [2].

$$N_o = \frac{N_F}{1-\varepsilon} \tag{2.14}$$

However, bubble coalescence and collapse can occur in real foaming process. True nucleus density (N_o^*) should be greater than or equal to the estimated nucleus density ($N_o^* \geq N_o$).

2.3 Review of Foam Microstructure Characterization

Nowadays, true foam microstructure can be observed by 3D scan technology using a volume rendering technique used to display a 2D projection of a 3D discretely sampled data set, as produced by a microtomography scanner, and image segmentation to remove the unwanted structures from the image by adjusting volume-rendering parameters. Computed tomography scan and x-ray microtomography are useful techniques that can be applied to observe the foam microstructure. Then, cell dimensions and cell density can be measured.

2.3.1 Computed Tomography

Computed tomography (CT) is an imaging method using tomography created by computer processing. Digital geometry processing is used to generate a 3D image of the inside of an object from a large series of 2D X-ray images. The CT produces a volume of data that can be manipulated, through a process to show various bodily structures based on their ability to block the X-ray beam. The images generated are in the axial or transverse plane, orthogonal to the long axis of the body, modern scanners allow this volume of data to be reformatted in various planes or even as 3D volumetric representations of structures. Many scanned data are progressively taken as the object is gradually passed through. Combining by mathematical procedures was known as tomographic reconstruction. This increases the resolution of each volume element known as Voxel. Then a Back Projection process essentially reverses the acquisition geometry and stores the result in another memory array. Then, this data can be displayed, photographed, or used as input for further processing [28].

2.3.2 X-Ray Microtomography

X-ray microtomography, imaging by sectioning, using waves of the x-ray energy. A device used in tomography is called a tomograph, while the image produced is a tomogram. X-rays is used to create cross-sections of a 3D-object that later can be used to recreate a virtual model without destroying the original model. The term micro is used to indicate that the pixel sizes of the cross-sections are in the micrometer range. These pixel sizes have resulted in the terminology micro-computed tomography, micro-computer tomography, high resolution x-ray tomography, and similar terminologies. Because microtomography scanners offer isotropic, or near isotropic, resolution of images does not need to be restricted to the conventional axial images [29].

Recently, M. D. Montminy *et al.* [30] used X-ray tomography and image processing technique to identify the actual foam structures of open-cell polyurethane foams (Figure 2.10A), including mean geometric parameters such as cell size, area of cell, and interior angle. Youssef and Maire [31, 32] used the same technique to make a 3D solid model (Figure 2.10B), and this 3D model was applied to finite element analysis to calculate effective properties.

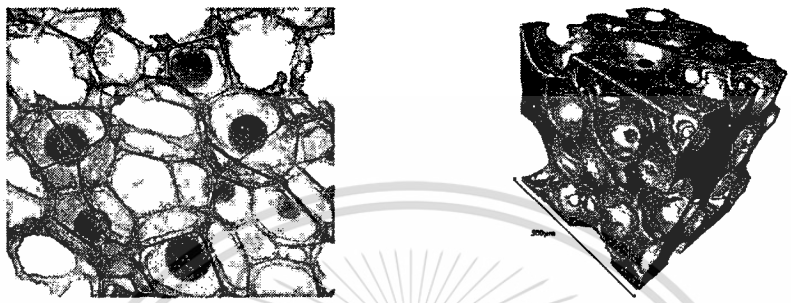

(A) (B)

Figure 2.10 (A) 3D image from X-ray tomography [25] (B) 3D model from CT technique [30].

2.4 Review of Existing Methods of Cell Density Estimation

In section 2.5, the techniques for observation of real cell microstructure were introduced. However, since cost of operation in measurement is quite expensive, the simple methods of estimation of cell density are preferred. Currently, the existing favorite methods of estimating cell density are the stereological simple average method, material balance-based method, and the cell density estimation of non-isotropic foams.

2.4.1 Stereological Simple Average Method

The stereological simple average method for estimation of cell density of polymeric foams is simple and rough. This simple equation was developed by simple stereological procedure and used widely as the conventional model of estimating cell density in isotropic foams. The estimation of cell density uses the 2D surface cell density (N_S) as parameter that can be observed from a single cross-sectional side from micrograph, as expressed in Equation (2.15)

$$N_F = [N_S]^{\frac{3}{2}} \tag{2.15}$$

The stereological simple average method simple average method is appropriate to uniform isotropic foams. The foam in question may be uniform or non-uniform dispersion.

2.4.2 Material Balance-Based Method

Material balance based model also is convenient for characterization of cell density, with the material balance-based method being the most reliable including important parameters: volume expansion ratio (ϕ) and average cell size (d).

Cell density refers to the number of cells (n_{cell}) in a unit volume of foam, as expressed in Equation (2.16).

$$N_F = \frac{n_{cell}}{V_T} \tag{2.16}$$

The number of cells equals the total volume of gas bubbles divided by the volume of a unit bubble (V_{bb}) as expressed in Equation (2.17).

$$n_{cell} = \frac{V_G}{V_{bb}} \tag{2.17}$$

Equation (2.17) can be written as Equation (2.18).

$$N_F = \frac{1}{V_T}\left(\frac{V_G}{V_{bb}}\right) \tag{2.18}$$

Substituting V_G from Equation (2.6) into (2.18) gives Equation (2.19).

$$N_F = \frac{1}{V_{bb}}\left(\frac{V_T - V_P}{V_T}\right) \tag{2.19}$$

Combining Equations (2.3) and (2.19) leads to the general form of the material balance-based cell density model, as shown in Equation (2.20) [9].

$$N_F = \frac{1}{V_{bb}}\left(1 - \frac{1}{\phi}\right) \tag{2.20}$$

The volume of a unit gas bubble (V_{bb}) is dependent on the bubble shape of foams. For spherical bubble foams, V_{bb} can be calculated by Equation (2.21).

$$V_{bb} = \frac{\pi d^3}{6} \tag{2.21}$$

On the other hand, in the case of ellipsoidal bubble foams with idealized dimension of longituditional axis of L, primary and secondary transversal axes of B and W, respectively, as seen in Figure 2.11, V_{bb} can be expressed by Equation (2.22).

$$V_{bb} = \frac{\pi WBL}{6} \tag{2.22}$$

In practice, analysis of foam morphology from micrograph is two-dimensional analysis. The simple way to analyze is to approximate L≈B. Volume of a unit gas bubble can be calculated by Equation (2.23).

$$V_{bb} = \frac{\pi WB^2}{6} \tag{2.23}$$

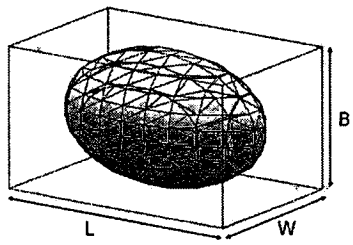

Figure 2.11 Dimension of an ellipsoidal bubble [9].

At present, the true cell densities of polymeric foams are still not well estimated, with the material balance-based method being the most reliable.

2.4.3 Cell Density Estimation of Non-isotropic Foams

R. Gosselin and P. Jerschew [9] introduced the method to estimate cell density of ellipsoidal foams with non-isotropic distribution or inhomogeneity, such as extruded foams, using surface cell density of two perpendicular cross-sections: longituditional direction (N_1) and transversal direction (N_2), as shown in Figure 2.12. The shape of ellipsoidal bubbles is assumed to be spherical in longituditional cross-section (B=W) in Figure 2.11. Cell density of ellipsoidal foam can be estimated by Equation (2.24).

$$N_F = N_1 (N_2)^{\frac{1}{2}} \tag{2.24}$$

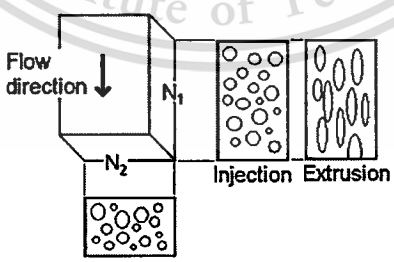

Figure 2.12 Observation of two perpendicular cross-sections [9].

In addition, this estimating method is concerned with non-uniform distribution of two perpendicular directions. The estimating results using this method are similar to material balance-based method [9]. However, the difficulty of preparation of perpendicular samples for morphological study is the main problem for this method.

2.4.4 Comparison of various estimating methods

The estimations of cell density using various methods are compared in Table 2.1. True cell density of foam cannot be investigated by traditional techniques. The true cell densities of polymeric foams are still not well-estimated, with the material balance-based method being the most reliable due to the principle of material balance. However, simple averaging method is usually used for polyhedral foams. The true cell densities of microcellular foams are still being not well-estimated, with the material balance-based method being the most reliable. Both the material balance-based and conventional models give similar results for high density polymeric foams [9], while the different models do not give similar results for low density isotropic foams. However, in case of irregular or complex shapes of gas bubbles, the estimation by material balance-based cell density method is difficult to define the sizes of gas bubbles.

Table 2.1 Comparison of various methods for estimation of cell density.

Method	Conventional stereological simple averaging	Material balance	Perpendicular stereology
Equation	Equation (2.15)	Equation (2.20)	Equation (2.24)
Based principle	stereology	material balance	stereology
Number of Parameters	1	3	2
Morphology parameter	N_S or $\bar{A}$	d	N_{S1}, N_{S2}
Bulk Density parameter	-	ρ_F, ρ_P	-
Application for closed-cell	Available	Available	Available
Application for open-cell	Available	Not available	Available
Application for spherical bubble	Available	Available	Available
Application for ellipsoidal bubble	Not available	Available	Available
Assumption of bubble distribution	uniform in 3D	Uniform or non-uniform	Uniform in 2D
Advantage	Easy to estimate with simple average method	Good for spherical bubble	Good for both isotropic and non-isotropic foams
Limitation	Poor for non-isotropic foams	Poor for non-isotropic foams	Difficult of perpendicular samples preparation
Reliability	Fair	Good	Good

2.5 Review of Space-Occupied Analysis

Space-occupied analysis is used to examine occupying area or volume of distributed objects in 2D or 3D spaces such as voronoi tessellation method of constructing polygonal or polyhedral cells of points, circles, and spheres [33-35], as shown in Figure 2.13. The space-occupied analysis is also applied to the analysis of area-occupied or volume-occupied of the foam bubbles, investigation of the cell structure and cell boundary of polymeric foams from the cross-section observed from micrograph, and analysis of the cell shapes of various atomic packing structures [36-38]. The idea of space-occupied analysis inspires this work to estimate cell density by analyzing cell boundary of periodic foam structure, i.e., cell shape and cell size, which is independent to bubble shape, bubble size, or foam processing, for both post-production isotropic high density and low density closed-cell foams.

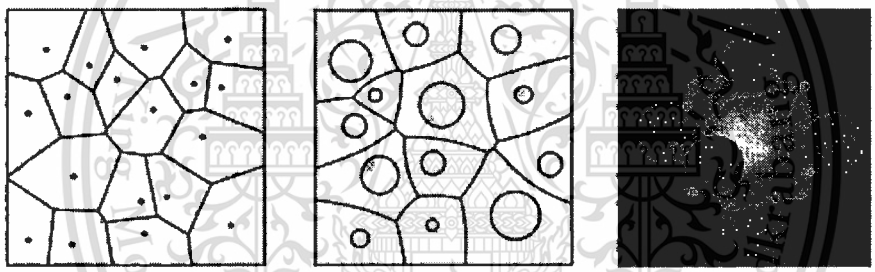

Figure 2.13 Voronoi diagrams of (A) points, (B) circles, and (C) spheres sets [17].

The structure of foam, shape of a unit cell, and the cell cross-section are main factors of the estimation of cell density by analyzing cell boundary of periodic foam structure. Polymeric closed-cell foams are typically pentagonal dodecahedral cells [39-40]. In analyses of transport phenomena and finite element, perfect cell cross-sections, i.e., regular tetragonal cells or regular hexagonal cells were used [41-43]. However, generally, morphologies of polymeric foams observed in micrographs displayed non-perfect cross-sections, which are usually pentagonal, hexagonal or square, and are variously distorted with a non-uniform cell size and random cell distribution [39]; the cell cross-sections cannot represent their information in 3D.

2.6 Background in Atomic Packing Structure Model

Atomic packing structure model [44] describes the orientation of atoms in crystal structure. The unit cell is the smallest structure that repeats itself by translation through the crystal. We construct these symmetrical units with the hard spheres. The most common types of unit cells are the faced-centered cubic (FCC), the body-centered cubic (BCC) and the hexagonal close-packed (HCP). Other types exist particularly among minerals. The simple cubic (SC) is often for didactical purpose, but no material really has this structure. Unit cells of various atomic packing structures are shown in Figure 2.14.

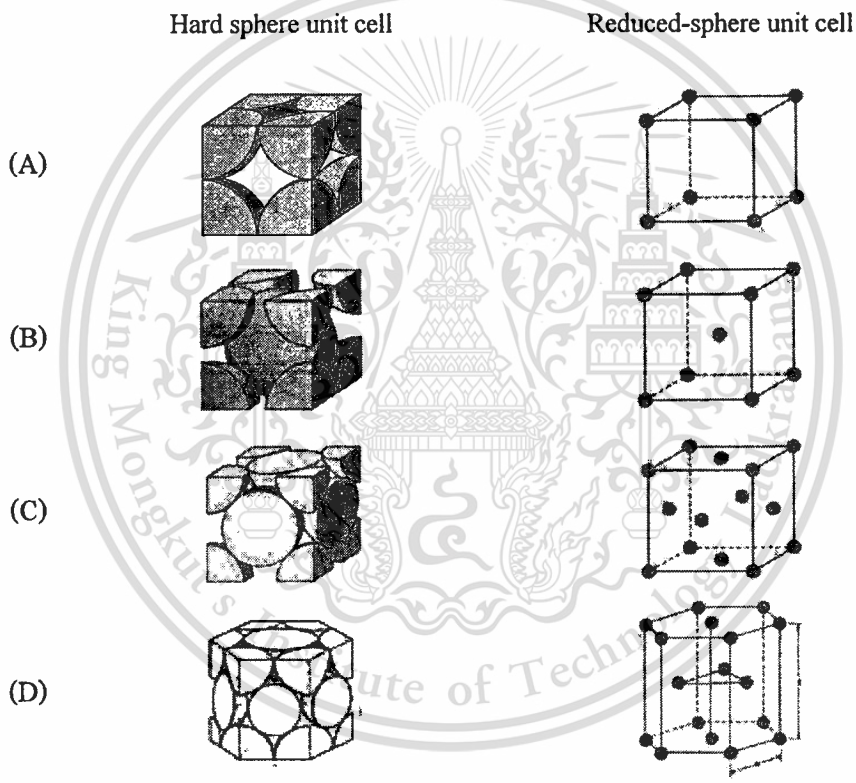

Figure 2.14 Unit cells of variuos atomic packing structures [44].

Two important characteristics of a crystal structure are the coordination number and the atomic packing factor (APF). For metals, each atom has the same number of nearest neighbor or touching atoms, which is the coordination number. The APF is the fraction of solid sphere volume in a unit cell [44], as expressed in Equation (2.25).

$$\text{APF} = \frac{\text{volume of atoms in a unit cell}}{\text{total unit cell volume}} \tag{2.25}$$

Coordinate numbers and APFs of various crystal structures are shown in Table 2.2.

Table 2.2 Unit cells of various atomic packing and their parameters [44].

Unit cell	Coordination number	APF
Simple cubic	6	0.5236
Body-centered cubic	8	0.6802
Face-centered cubic	12	0.7404
Hexagonal closed packed	12	0.7404

2.7 Foam Microstructure Models

2.7.1 3D Cellular Structure Models

Foam structure model is a 3D periodic cell frameworks used to describe microstructure of foam cells. The shape of cells in foam microstructure is a regular polygon as in (Figure 2.5), dependent on its cell packing structure [45]. Furthermore, 3D foam microstructure model is used in finite element analysis to study mechanical properties of the foam. It translates the non-periodic real foam model into periodic element based on idealized unit cells, also called repeating unit, as shown in Figure 2.15.

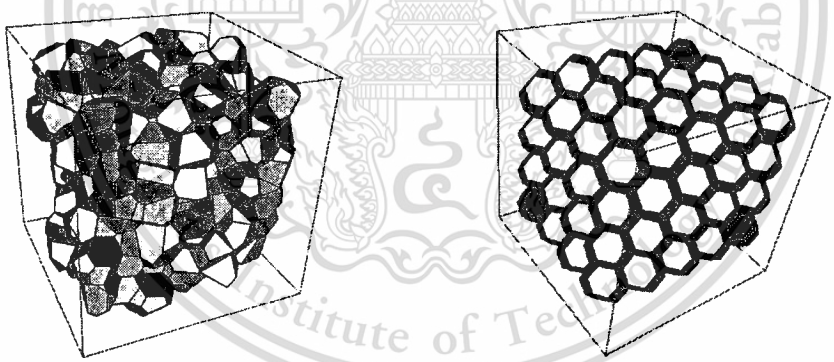

(A) (B)

Figure 2.15 Simulation of (A) random foam and (B) uniformed tetrakaidecahedron structure [45].

V. Shulmeister *et al.* [1] has modeled a foam microstructure as 3D frameworks of cell struts. The initial distribution of the nuclei completely determines the original geometry of the Voronoi tessellation and, hence, the strut framework. To create a regular space-filling cell framework, a regular BCC packing of tetrakaidecahedron cells and a regular FCC packing of tetrakaidecahedron rhombic dodecahedron cells packed distribution of nuclei are raised as examples here, as displayed in Figures 2.16.

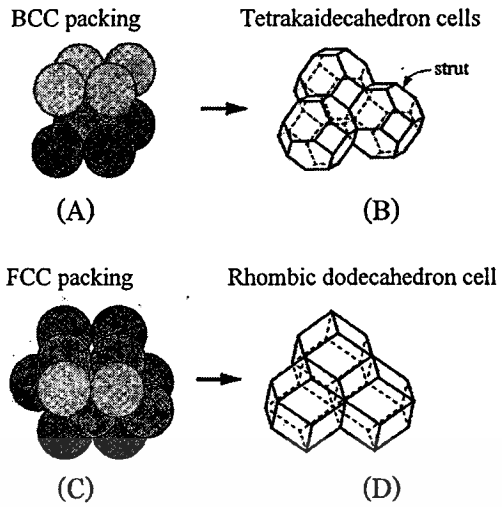

Figure 2.16 (A) Tetrakaidecahedron based on body-centered cubic (BCC) distribution of nuclei and (B) its subsequent strut framework. (C) Rhombic dodecahedron based on a face-centered cubic (FCC) closest nuclei distribution and (D) its subsequent strut framework [1].

Similarity of periodic packing structure between atomic packing and cellular microstructure can be shown in Table 2.3.

Table 2.1 Similarity of periodic structure between atomic packing and cellular microstructure.

Packing structure	Repeating unit cell of cellular microstructure
SC	Regular Hexahedron (simple cubic)
BCC	Tetrakaidecahedron (Kelvin foam), regular octahedron
FCC	Rhombic dodecahedron, pentagonal dodecahedron

Recently, unit cell models have proven to be useful theoretical tools for understanding some of the key aspects of the mechanical behavior of cellular solids such as the dependence of failure properties on relative density and on the failure mode of individual cells. In contrast to an idealized unit cell, most cellular materials have inherent imperfections and inhomogeneities in their microstructure [46].

2.7.2 2D Cellular Structure Models and Cell Cross-Sections

Two-dimensional cell model was used to describe cellular microstructure using cell cross-sectional windows. Generally, random cell microstructures appear on micrographs, as seen in Figure 2.17A. Simply periodic cell microstructure with repeating unit, such as tetragonal or hexagonal cells, as shown in Figure 2.17B, can be used to model and to simulate the transport phenomena of foaming process and 2D finite element analysis as well as 3D analysis [27, 46].

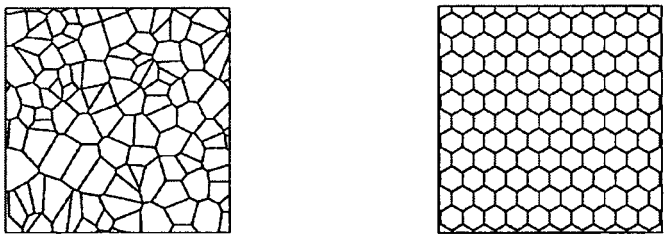

Figure 2.17 Two-dimensional cellular structure models of (A) a realistic random microstructure and (B) a periodic hexagon microstructure [27].

In order to analyze the cross-sections of idealized periodic microstructures, perfect cross-sections are used as useful theoretical tools for analysis. The shape of repeating unit cell windows depends on the assumption of 3D microstructure; regular tetragonal cell window for simple cubic microstructure, and regular hexagonal cell window for tetrakaidecahedral or dodecahedral microstructure, as shown in Figure 2.18.

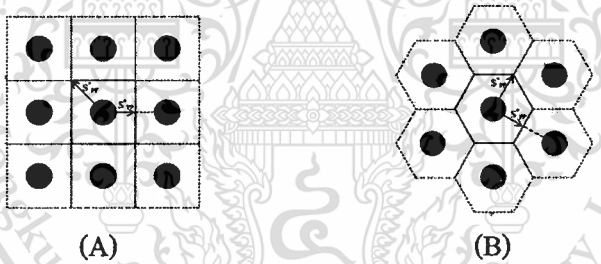

Figure 2.18 Two-dimensional periodic structures of (A) tetragonal and (B) hexagonal cells [41].

On the other hand, cell cross-sectional windows usually vary from perfect cross-sectional windows as non-perfect cross-sections. In a previous study, K. Li *et al.* [42] presented effects of cell shape and cell cross-sectional area variations on the elastic properties of 3D open-cell foams. K. M. Lewis *et al.* [39] presented a reliable mathematical relationship between the observed cell cross-sectional window area and the average cell size, which has allowed the realization of useful correlations for low density closed-cell foams. The observed cell windows were usually pentagonal, hexagonal or square and were variously distorted, and all the cells were assumed dodecahedral. The average cell diameter was calculated by the following Equation (2.26) [39].

$$D_C = 2.1354\left(\overline{A}\right)^{\frac{1}{2}} \tag{2.26}$$

In considering a periodic cell microstructure, cell cross-sectional windows model can be applied to describe the cell microstructure, which was either perfect or non-perfect cross-section of the foam structure.

Chapter 3

Mathematical Models

This chapter describes a comprehensive research on development of the mathematical models in two parts: Part 1 describes how the estimation of cell density with critical bubble lattice method developed, and Part 2 introduces the characterization of isotropic foam behavior with the newly-developed isotropic foam index.

Part 1 Estimation of Cell Density using Principle of Critical Bubble Lattice

This part introduces how newly mathematical models was developed. First, the overview of the development was introduced. Then, the principle of bubble rearrangement, the definition of critical bubble and the concepts of critical bubble lattice model were introduced by representing atomic packing structure. Analysis of variation of determined cell sizes with perfect and non-perfect cell cross-sections was taken into account. Material balance-based cell density was derived. Finally, estimation of material balance-based cell density using critical bubble lattice for master equations are presented.

3.1 Overview of Mathematical Model Development

In this study, three previous physical models were studied: atomic packing model, 3D foam structure model, and cell cross-sectional windows model. The integration of these models was applied to develop a mathematical model for estimation of cell density of polymeric foams. Figure 3.1 illustrates briefly how the mathematical model of cell density estimation using surface cell density was developed. Solid-line blocks refer to recent models and dash-line blocks refer to developed parts. First, the general form of the relationship between cell density and cell size with function f_1 was presented by utilize of the newly-developed critical bubble lattice model that associates foam structures with atomic packing structure models. Second, the general form of the relationship between cell size and average cell cross-sectional windows area with function f_2 was introduced. Finally, mathematics led these general forms to the master equation of cell density estimation with surface cell density.

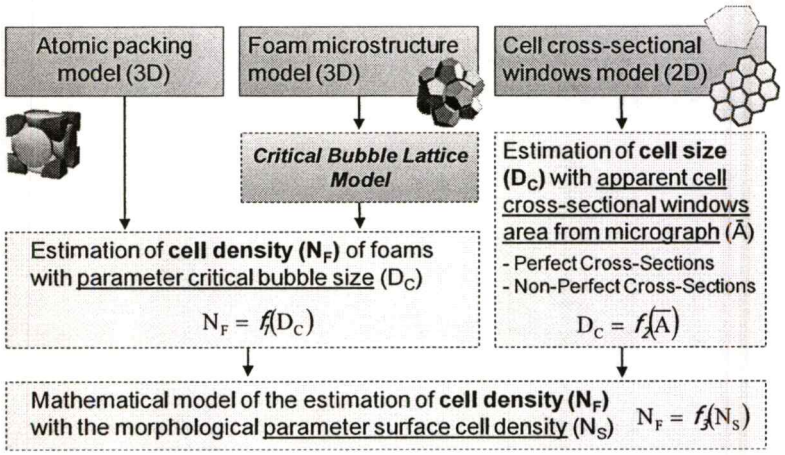

Figure 3.1 Integrating methodology of development of models for estimation of cell density.

At present, modeling of 3D structure of polymeric foams was studied wildly to describe cell morphology such as bubble shapes and average cell size, to study transport phenomena in foaming process, and to analyze mechanical properties of foamed materials with finite element method. In this study, comparison between atomic packed structure and 3D foam structure at cell structure and cell shape was studied. Critical bubble lattice model was then presented in association of the foam structure of pentagonal dodecahedron (12-hedron) cells with face-centered cubic (FCC) atomic packed structure.

3.2 Principle of Bubble Rearrangement

Generally, bubbles grow in all directions from random initiated nuclei, and gas bubbles are dispersion randomly. The concept of bubble rearrangement rearranges randomly dispersed gas bubbles into periodic structure pattern to simplify the methods of estimating cell density with analysis of comfortable periodic structure. The same number of bubbles dispersed in the same volume of foams or the same area of interest size led to the same cell number density; with independent to bubble sizes, bubble shapes, or initial co-ordinate of dispersed bubbles; no change in their cell density, as shown in Figure 3.2.

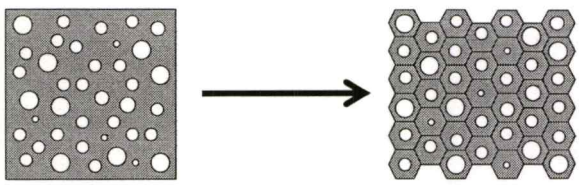

Figure 3.2 Rearrangement of (A) thirty-nine random dispersed bubbles into (B) periodic volume-equivalent hexagonal cell cavities, at the same area of interest size.

3.3 Principle of Critical Bubble Lattice

In this section, the estimation of cell density using the critical bubble lattice method is introduced to show how the analysis of cell structure can be used as the estimation of cell density with independent of gas bubbles inside. Finally, the master equation for the estimation of cell density with the critical bubble lattice was presented.

3.3.1 Definition of Critical Bubble

Critical bubbles are assumed the largest pseudo spherical gas bubbles that expand full filling the isotropic cell cavities as shown in Figure 3.3.

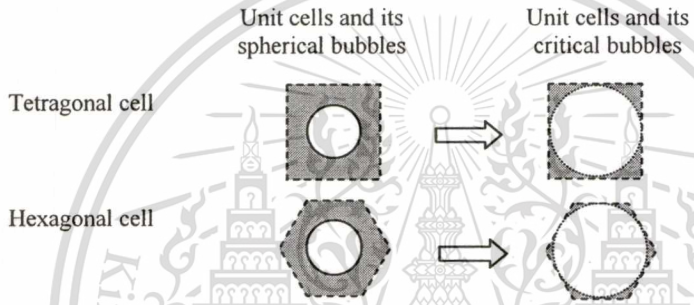

Figure 3.3 Cell cross-sectional windows with their bubbles.

3.3.2 Similarities between Atomic Packing Structure and Critical Bubble Lattice

The critical bubble lattice model was developed to describe uniform distribution of gas bubbles in a periodic structure. The similarities between the critical bubble lattice and an atomic packed structure were studied. The geometric properties of atomic packing were applied to estimate the properties of the critical bubble lattice; for instance, the void fraction of the critical bubbles equals the atomic packing factor (APF), and the cell density of both the critical bubble lattice and an atomic packed structure are equal. The similarities between the atomic packing model and the critical bubble lattice model are shown in Table 3.1.

Table 3.1 Similarities between an atomic packed structure and the critical bubble lattice.

Property	Atomic packed structure	Critical bubble lattice
Packing	Spherical solid atoms in void space	Spherical gas bubbles in polymeric resin
Volume fraction	APF, volume fraction of solid spheres in unit cell and total volume of unit cell	Void Fraction, fraction of spherical bubble in unit cell and total volume of unit cell
Cell density	Number of solid spheres per unit volume of cell	Number of critical bubble spheres per unit volume of cell

In brief, the critical bubble lattice explains the periodic packing structure of the critical bubbles, similar to an atomic packed structure. This structure may be simple cubic (SC), body-centered cubic (BCC), or face-centered cubic (FCC) packing. The cell cavities of low density isotropic polymeric foams are typically pentagonal dodecahedral which its critical bubble lattice are packed similarly to the FCC atomic packing structure, as shown in Figure 3.4.

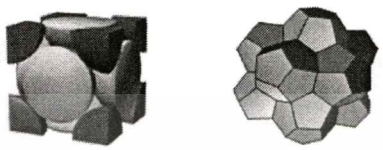

(A) (B)

Figure 3.4 Schematic of (A) FCC atomic packing structure and (B) pentagonal dodecahedron foam structure.

3.3.3 Identical Cell Density at the Same Cell Size

The concept of the critical bubble lattice introduces a useful principle for characterizing the cell density independently from bubble shape or size. Figure 5 shows three identical cell size foams are compared: uniform spherical, critical, and non-uniform bubbles, all foams are the same cell size but their bubbles are different in shapes and sizes. It was shown that all of the foam in Figure 3.5 could be represent the same critical bubbles as seen Figure 3.5B; the size of critical bubbles signifies only the cell size. Moreover, these foams should have the same cell density because these have the same cell boundary, independently from shape or size of the bubbles.

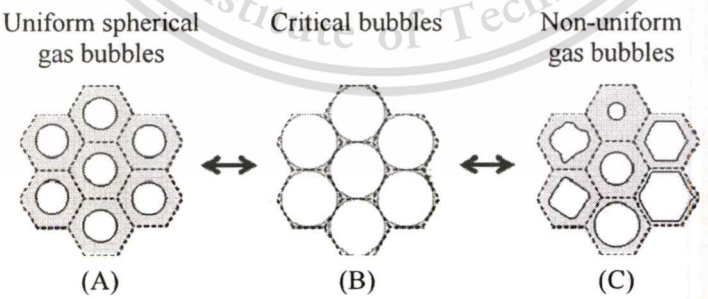

Figure 3.5 Identical hexagonal cells and the gas bubbles contained therein.

Furthermore, the cell density is identical at the same cell size, independent of gas bubbles. The cell density of any uniform or non-uniform gas bubbles inside the same cell structure are similar to the cell density of the critical bubble lattice ($N_{F,CR}$), as expressed in Equation (3.1).

$$N_F = N_{F,CR} \quad (3.1)$$

In practice, void fractions (ε) were taken from the APFs of atomic packed structures, while expansion ratios (ϕ) were calculated with these void fractions, as in Equation (2.7).

$$\phi = \frac{1}{1-\varepsilon} \tag{2.7}$$

The theoretical limit of expansion in terms of critical void fraction (ε_{CR}) and critical expansion ratio (ϕ_{CR}) of various cell structures can be shown in Table 3.2.

Table 3.2 Various cell structures and their theoretical limit of spherical expansion parameters [3].

Lattice	Shape of Unit Cell	ε_{CR} (-)	ϕ_{CR} (-)
SC	Cubic	0.5236	2.0991
BCC	Tetrakaidecahedron (Kelvin foam)	0.6802	3.1270
FCC	Pentagonal dodecahedron (12-Hedron)	0.7404	3.8521

3.3.4 Material Balance-Based Cell Density Model using the Critical Bubble Lattice

In order to determine the material balance-based cell density of various foams, both spherical and polyhedral bubbles must be examined. The combination of material balance-based cell density in Equations (2.22) and (2.23) and critical bubble lattice model leads to:

$$N_F = \frac{1}{V_{bb}}\left(1-\frac{1}{\phi}\right) \tag{2.22}$$

$$V_{bb} = \frac{\pi d^3}{6} \tag{2.23}$$

It can be written in Equation (3.2).

$$N_F = \frac{6}{\pi (D_C)^3}\left(1-\frac{1}{\phi_{CR}}\right) \tag{3.2}$$

In Equation (3.2), the value of the critical expansion ratio was obtained from Table 3.2, which depends on the packing structure. Therefore, the general form of the cell density of atomic packed structures with a new parameter, the periodic factor (α), is given in Equation (3.3).

$$N_F = \frac{\alpha}{(D_C)^3} \tag{3.3}$$

Various atomic packed structures and their periodic factors are summarized in Table 3.3.

Table 3.3 Various atomic packed structures and their geometric parameters.

Packed Structure	Shape of unit cell	Periodic factor, α (-)
SC	Cubic	1
BCC	Tetrakaidecahedron (Kelvin foam)	1.2990
FCC	Pentagonal dodecahedron (12-Hedron)	1.4142

3.4 The Relationship between Cell Size and Average Cell Window Area

It is important to note that it is not possible to measure the cell size (D_c) directly from the micrographs. For this reason, the relationships between cell size and measurable parameters such as surface cell density or average cell cross-sectional window area are studied.

Generally, the morphology of polymeric foams observed in micrographs displays non-perfect cross-sections with a non-uniform cell size and random cell structures, as shown in Figure 3.6A-B. In order to determine cell size from the perfect or non-perfect cross-sections, the relationship between the reference critical bubble size and the average cell cross-sectional windows area was studied. The average cell cross-sectional window area ($\bar{A}$), which represents the overall area of interest (A) divided by the number of cells (n), is expressed in Equation (3.4).

$$\bar{A} = \frac{A}{n} \tag{3.4}$$

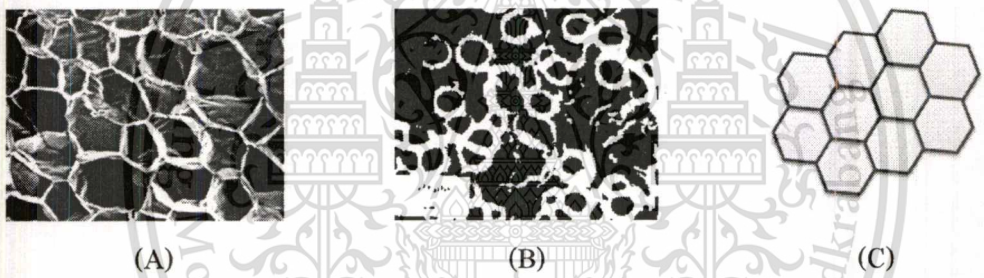

(A) (B) (C)

Figure 3.6 Cell cross-sections of (A) low density foams [6] and (B) high density foams from micrographs [11]; (C) perfect hexagonal cell windows.

The relationship between cell size and cell window area are studied in two cases: perfect and non-perfect cell cross-sections. For the perfect case, cell windows are hexagonal and fully cover their critical bubbles as shown in Figures 3.7 and 3.8A.

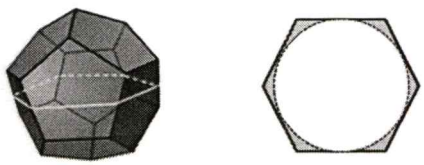

Figure 3.7 Schematic of (A) a pentagonal dodecahedral cell and its perfect cross-section, and (B) perfect cell cross-section and its critical bubble.

In reality, non-perfect cell cross-sectional windows are usually appeared in pentagonal, hexagonal or square are observed, as the dash-line windows presented in Figure 3.8B.

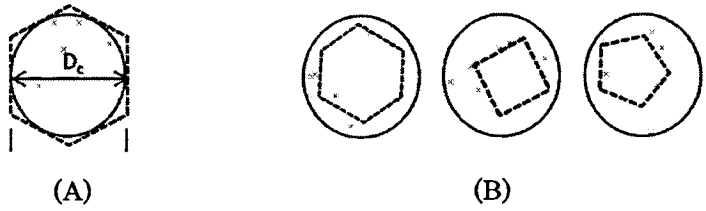

Figure 3.8 Apparent cell cross-sectional windows and their critical bubbles for (A) a perfect cell cross-section; (B) non-perfect cell cross-sections.

3.4.1 Perfect Cell Cross-Section

The perfect cell cross-sectional windows depend on the cell shape and foam structure such as tetragonal cross-sectional windows for regular cubic cells and hexagonal cross-sectional windows for pentagonal dodecahedral cells, as seen in Figures 3.5. In addition, the cell size is equal to the size of spherical cross-section of the critical bubble, as seen in Figure 3.8A.

To evaluate the relationship between cell size (D_C) and average cross-sectional cell window area ($\bar{A}$) of a hexagonal cell, six combined triangles of a hexagonal cell and its critical bubble were considered, as shown in Figure 3.9.

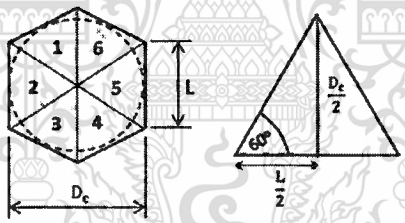

Figure 3.9 Schematic of a hexagonal cell window and its six combined equilateral triangles.

The relationship between D_C and L can be obtained by trigonometry from the equilateral triangle in Figure 3.9.

$$\tan 60^\circ = \frac{D_C/2}{L/2} \tag{3.5}$$

$$L = \frac{D_C}{\sqrt{3}} \tag{3.6}$$

The area of the hexagonal window is equal to the sum of the area of six combined equilateral triangles, as expressed in Equation (3.7).

$$\bar{A} = 6\left(\frac{1}{2}\right)\left(\frac{D_C}{2}\right)\left(\frac{D_C}{\sqrt{3}}\right) \tag{3.7}$$

Finally, the mathematical relationship between cell size and average cross-sectional cell window area for the perfect cross-section model was expressed in Equation (3.8).

$$D_C = 1.0746\left(\bar{A}\right)^{\frac{1}{2}} \tag{3.8}$$

3.4.2 Non-perfect Cell Cross-Section

In section 2.8.2, the reliable mathematical relationship between the observed cell cross-sectional window area and the average cell size was introduced in a work by K.M. Lewis *et al.* [39], which allow the realization of useful correlations for low density closed cell foams. The cell windows are usually pentagonal, hexagonal or square and are variously distorted, and all the cells are assumed dodecahedral. The average cell diameter is calculated by Equation (2.26).

$$D_C = 2.1354\left(\overline{A}\right)^{\frac{1}{2}} \tag{2.26}$$

3.4.3 The General Form of Mathematical Relationship between Cell Size and Average Cell Window Area

To simplify the analysis of the relationship between cell size and cell cross-sectional window area of either perfect or non-perfect cell cross-sectional windows from a micrograph, as shown in Equations (2.28) and (3.8), the mathematical relationship between cell size and average cell cross-sectional window area can be expressed with the apparent factor (κ), as seen in Equation (3.9).

$$D_C = \kappa\left(\overline{A}\right)^{\frac{1}{2}} \tag{3.9}$$

3.5 The General Form of the Model

The general forms of the estimation of cell density using cell size as a parameter by Equation (3.3) and the estimation of cell size with average cell cross-sectional window area by Equation (3.9) are combined. Then, the general form of the mathematical relationship between cell density and surface cell density of foam can be written with a new correcting factor, isotropic factor (φ), as expressed in Equation (3.10).

$$N_F = \varphi[N_S]^{\frac{3}{2}} \tag{3.10}$$

Where,

$$\varphi = \frac{\alpha}{\kappa^3} \tag{3.11}$$

The isotropic factor in Equation (3.10) also exhibits as the correcting factor to adjust the relationship between cell density and surface cell density for the conventional cell density model in Equation (2.15).

The mathematical model development of the estimation of cell density with the isotropic factor is summarized in Figure 3.10.

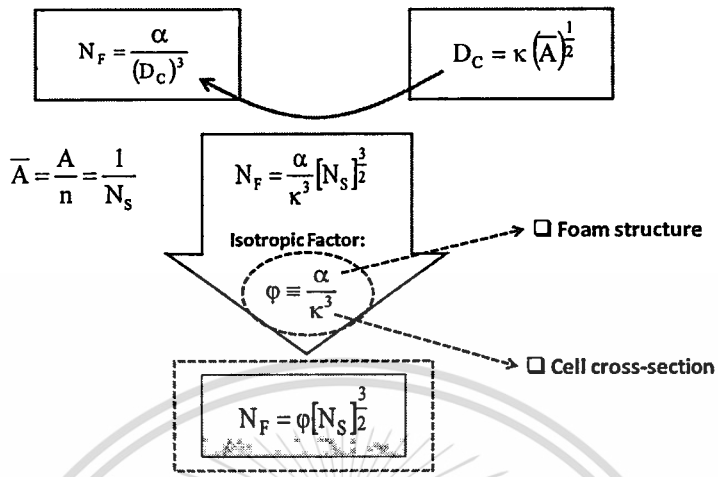

Figure 3.10 Summary of mathematical model development of cell density estimation.

3.6 Summary of Estimation of Cell Density using the Critical Bubble Lattice Method

1. The concept of bubble rearrangement is used to rearrange random dispersed gas bubbles into a periodic structure, for applying perfect cell cross-section model to the estimation of cell density of high density foam.

2. The critical bubble lattice model was developed to describe a uniform distribution of gas bubbles in a periodic structure. Similarities between the critical bubble lattice and an atomic packed structure were studied. A critical bubble is assumed to be the largest spherical gas bubble that could fulfill a cell cavity, as seen in Figures 3.5B. The geometric properties of atomic packing were applied to estimate the properties of the critical bubble lattice.

3. The unit cell is identical at the same cell size, as illustrated in Figure 3.5. Cell density of foam is independent from size or shape of bubbles inside. The general form of cell density estimation using the periodic factor (α) is shown in Equation (3.3). The value of periodic factor depends on cell structure, as shown in Table 3.3.

4. The relationships between cell size and measurable parameters such as surface cell density or average cell cross-sectional window area were studied. The general form of the mathematical relationship between cell size and average cell cross-sectional window area using apparent factor (κ) is expressed in Equation (3.9).

5. The general form of the mathematical relationship between cell density and surface cell density can be demonstrated by using isotropic factor (φ). The value of isotropic factor can be obtained from periodic factor (α) and apparent factor (κ), as seen in Equation (3.11). The isotropic factor also exhibits as the correcting factor for the conventional cell density model.

Part 2 Characterization of Isotropic Foam Behavior

This part introduces the characterization of isotropic foam behavior by comparing the foam in question with the standard isotropic foam.

3.7 Characterization of Isotropic Foam Behavior with Isotropic Foam Index

First, the definition of standard isotropic foam, standard isotropic foam factor, and standard isotropic cell density were introduced. Then, characterizing deviation of foam from the standard isotropic foam was introduced using isotropic foam index.

3.7.1 Standard Isotropic Cell Density and Standard Isotropic Factor

Standard isotropic foam refers to the perfect isotropic foam with one of various periodic structures. In the section 3.5, the general form of newly-developed model was introduced as shown in Equation (3.10). Likewise, the standard foam has the standard isotropic cell density (N_F°), as shown in Equation (3.12), which can be investigated by using surface cell density and a standard isotropic factor (φ_o).

$$N_F^\circ = \varphi_o [N_S]^{\frac{3}{2}} \tag{3.12}$$

The value of a standard isotropic factor depends on the standard isotropic factor and the natural of cell cross-sectional windows as the standard parameters, due to the foam morphologies such as high density foam, closed-cell low density foam, or open-cell foam.

3.7.2 Isotropic Foam Index

The isotropic foam index (η) is defined to indicate a deviation from the isotropic foam behavior, given as the logarithm of the ratio of the apparent isotropic factor (φ) and the standard isotropic factor (φ_o), as shown in Equation (3.13).

$$\eta = \log\left(\frac{\varphi}{\varphi_o}\right) \tag{3.13}$$

The standard isotropic factor φ_o in Equations (3.12) and (3.13) is dependent on the foam structure, and affects to the appearance foam morphology on a micrograph. This factor refers to the isotropic behavior of various foam structures. For complete isotropic foams, the isotropic foam index is equal to zero.

Combining of Equations (3.10), (3.12) and (3.13), the relationship between cell density and standard isotropic cell density can be written as in Equation (3.14).

$$N_F = 10^{\eta} N_F^{\circ} \tag{3.14}$$

In practice, the isotropic foam index can be evaluated by solving Equation (3.14), obtained by taking logarithm of the cell density in Equation (3.10) or material balance-based cell density divided by the standard isotropic cell density in Equation (3.12), as in Equation (3.15).

$$\eta = \log\left(\frac{N_F}{N_F^{\circ}}\right) \tag{3.15}$$

3.8 Summary of the Characterization of Isotropic Foam Behavior Using the Isotropic Foam Index

1. Standard isotropic foam refers to the structure that is perfect isotropic foam structure with one of various periodic structures.

2. Standard isotropic cell density (N_F°) is the cell density of the standard foams.

3. Standard isotropic factor (φ_o) is used for the estimation of isotropic foam using surface cell density as a parameter, and the value of standard isotropic factor depends on the cell structure or the appeared morphology from micrograph.

4. The isotropic foam index (η) was defined to indicate a deviation from the isotropic foam behavior, given as the logarithm of the ratio of apparent isotropic factor (φ) and standard isotropic factor (φ_o). In practice, the isotropic foam index can be evaluated by Equation (3.15).

Chapter 4

Modeling and Validation of Models

This chapter describes a research conducted to achieve pentagonal dodecahedral foam structured in FCC lattice with perfect cross-section (FCC-PF) and non-perfect cross-section (FCC-NPF) models, as a case of examples, to describe precisely the effect of non-perfect cell cross-section that can occur in realistic on cell density determination of high density and low density foams. Then, the experimental data sources and methods of analyses were described and compared with results from the model.

4.1 Models

The new-developed model of the cell density estimation in Equation (3.10) is used to investigate the effect of non-perfect cell cross-section on the cell density estimation of pentagonal dodecahedral foams in two cases: first, based on the FCC lattice with perfect cross-sectional windows (FCC-PF), and, second, based on the FCC lattice with non-perfect cross-sectional windows (FCC-NPF). The parameters of each model were summarized and calculated from Equations (3.3), (2.28), (3.9) and (3.11), as shown in Table 4.1.

Table 4.1 Conventional and newly developed models and their parameters.

Model	Foam structure		Cell cross-section		Isotropic Factor (φ)
	Assumption	Periodic factor (α)	Assumption	Apparent factor (κ)	
Conventional model	-	-	-	-	1
FCC-PF	FCC lattice	1.4142	Perfect cross-section	1.0746	1.1398
FCC-NPF	FCC lattice	1.4142	Non-perfect cross-section	2.1354	0.1453

4.1.1 Cell Densities of Low Density Foams

Because the cell cross-sections of low density closed-cell foams may appear uncertainly within perfect and non-perfect cross-sections, cell densities of low density foams should be between FCC-PF and FCC-NPF models, the plot between surface cell density and surface cell density shows the isotropic foam region for low density foam, the region between the values those calculated by the FCC-PF and FCC-NPF models, as seen in Figure 4.1.

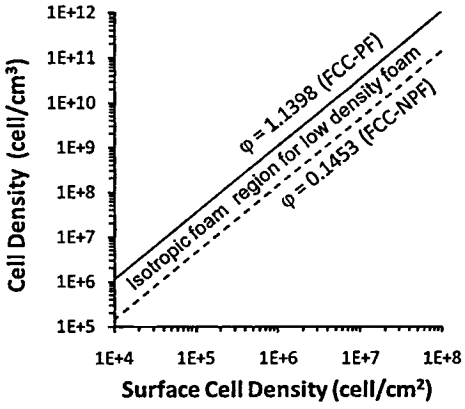

Figure 4.1 Plot of cell density at surface cell density and theoretical isotropic foam region for isotropic low density foams.

4.1.2 Cell Densities of High Density Foams

According to the experiment in recent work by R. Gosselin and P. Jerschew (2005) as discussed in the section 1.1, material balance-based and conventional simple average models have shown the similar result of cell density. Therefore, isotropic factor (φ) should be near to 1; therefore, prefect cross-section model (FCC-PF) can be used in the estimate cell density of high density foams. In case of high density foams, the rearrangement of the random distribution of the spherical bubbles into a periodic pattern of hexagonal cells is considered to simplify the analysis. In reality, bubbles grow from the nuclei dispersed in the polymer matrix until contact with neighboring bubbles causing their transformation from spherical bubbles into polyhedral cavities. The rearrangement of random nuclei (Figure 4.2A) into a periodic pattern is performed before the bubble growth step (Figures 4.2B-4.2D), with the assumption that no deflation or collapse of the bubbles occurs. For this assumption, the number of nuclei and the number of cells should be equal; in other words, the cell densities of randomly dispersed spherical bubbles and periodic structured bubbles inside the same cavities of interest should be equal.

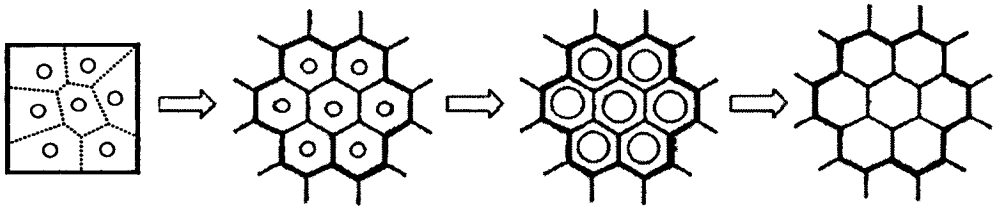

Figure 4.2 Distribution of gas bubbles in the same cell cavities of interest: (A) random dispersed spherical bubbles, (B) rearranged bubbles in periodic cavities of 2D hexagonal cells, (C) spherical bubble growth, and (D) polyhedral bubbles completely filling the cell cavities.

The cells are typically pentagonal dodecahedral cavities and the periodic pattern of the nuclei and the bubbles is the FCC lattice. Thus, the 2D hexagonal cells model can be used to represent the cell boundaries, similar to the FCC-PF model.

4.2 Methodology for Validation of Models

This section describes how to test and validate the new-developed model. Extracted essential parameters from published data that used in the calculations of material balance-based cell density, i.e., cell size, expansion ratio, and surface cell density, were used to test the theoretical maximum limit of the estimation of cell density using FCC lattice model, to test the range of estimation between FCC-PF and FCC-NPF models, and to investigate the standard isotropic foam factors for isotropic high density and isotropic low density foams, as described below.

4.2.1 The Collection of Recently Published Data

The collection of published data presents the published data. These data were used to extract the essential parameters in analysis, i.e., surface cell density, average bubble size, and expansion ratio. The recently published data of interest are collected for high density and low density foams both microcellular and conventional scale as follows:

1) Microcellular foams:

1.1) Low density microcellular foams:

(1) Polyethersulfone foams, H. Sun *et al.* (2000) [47].

(2) Polyphenylsulfone foams, H. Sun *et al.* (2000) [47].

1.2) High density microcellular foams:

(1) Acrylonitrile-butadiene-styrene foams, E. Murray *et al.* (2000) [48].

(2) Polyvinylchloride foams, V. Kumar and J. Weller (1993) [49].

(3) Polycarbonate foams, V. Kumar and J. Weller (1994) [50].

2) Conventional foams:

2.1) Low density conventional foams:

(1) Polystyrene foams, P. Srichay and P. Methakul (2005) [51].

2.2) High density conventional foams:

(1) Polypropylene foams, P. Spitael and C. W. Macosko (2004) [52].

4.2.2 Extracted Parameters from Available Published Data

Generally, recently studies reported their experimental data in terms of density of polymer, density of foam, and nucleus density. In this work, volume expansion ratio and surface cell density are required for the calculation of material balance-based and conventional stereological cell densities.

1) Volume Expansion ratio

Volume expansion ratio is calculated from the ratio between density of polymer and density of foams as the inverse of relative density. Volume expansion ratio of foam was investigated by the ratio of densities of polymer and foam in Equation (2.4).

$$\phi = \frac{\rho_P}{\rho_F} \tag{2.4}$$

Alternatively, the inverse of relative density can be applied to calculate volume expansion ratio, as shown in Equation (2.5).

$$\phi = \frac{1}{R_F} \tag{2.5}$$

2) Evaluation of Extracted Surface Density

The nucleus densities reported in recently published data are calculated by Equations (2.13) or (2.14).

$$N_o = N_F \phi \tag{2.13}$$

$$N_o = \frac{N_F}{1-\varepsilon} \tag{2.14}$$

Where, stereological cell density (N_F) can be calculated by Equation (2.15).

$$N_F = [N_S]^{\frac{3}{2}} \tag{2.15}$$

Thus, this study extracts the surface cell density (N_S) using the Equation (4.2).

$$N_S = \left[\frac{N_o}{\phi}\right]^{\frac{2}{3}} \tag{4.2}$$

4.2.3 Estimation of True Cell Density

Material balance-based cell density calculated by Equation (3.9) was applied to estimate true cell density, and plotted in the scattering plot of cell densities versus surface cell densities. The cell density of foam was calculated using the material balance based-model, which

calculates with parameters average apparent bubble size and apparent volume expansion ratio, as shown in Equation (4.3).

$$N_F = \frac{\pi d^3}{6}\left(1-\frac{1}{\phi}\right) \tag{4.3}$$

4.2.4 Method of Analysis for Testing and Validation of the Models

Testing and validation of the models is to test the theoretical maximum limit of the estimation of cell density using FCC lattice model, to test the range of estimation between FCC-PF and FCC-NPF models, and to investigate the standard isotropic foam factors for isotropic high density and isotropic low density foams, as described below.

1) Plot the Relationship between Cell Density and Average Cell Size

The plot of cell density versus average cell size is perform in semi-logarithm scale to study the FCC lattice as theoretical maximum limit of estimation. The cell density in the scattering plot is material balance-based cell density as described in section 4.2.1, while average cell size is perfect cross-sectional cell size which calculated by Equation (4.1).

2) Plot the Relationship between Cell Density and Surface Cell Density

The plot of cell density versus surface cell density is perform in logarithm scale to study of the theoretical range of estimation using new-developed model and its validation for the sample models: FCC-PF and FCC-NPF. The cell density in the scattering plot was material balance-based cell density as described in section 4.2.1. Surface cell density is extracted from conventional cell density or nucleus density from recently published data.

3) Investigation of Standard Isotropic Factor

The data of microcellular high density and microcellular low density foams were collected to investigate the standard isotropic factors of isotropic high density and isotropic low density foams. The investigation was performed by analyzing the scattering plot of cell density versus surface cell density, as in section 4.2.3. Then, percentage average absolute deviation (%ADD) was used to measure the accuracy of the models by measuring the deviation of the calculation by the model (x_{calc}) from experimental data (x_{exp}), as calculate by Equation (4.1).

$$\%AAD = \left|\frac{x_{exp} - x_{calc}}{x_{exp}}\right| \times 100 \tag{4.1}$$

A model which has lower %ADD is better accuracy and appropriate to be a standard isotropic factors for high density or low density foams.

4.3 Experimental Procedure

Two experiments for characterization of isotropic foams and non-isotropic foams were set-up and results are predicted by the new-developed model. Polyethylene foams were prepared for the case of isotropic foams, and sisal fiber/polypropylene composite foams was prepared for non-isotropic foams. Preparations of the foam samples are described below.

4.3.1 Preparation of Polyethylene Foam Samples

Polymer blends consist of two based polymer from Thai Polyethylene co., ltd. : (a) polymer-A has melting temperature of 135 °C bulk density 0.954 g/cm^3, and (b) polymer-B has melting temperature of 140 °C bulk density 0.949 g/cm^3. Both grades of polymer are mixed with nucleating agent by extruder at 150 °C to produce polymer blend pellets, with different compositions as shown in Table 4.2. The polymer blends are foamed in high pressure vessel of 12 MPa at 250°C with oil-bath temperature control by using foaming apparatus as explained in section 4.3.3.

Table 4.2 Compositions of polymer blends.

Sample	Polymer-A (wt%)	Polymer-B (wt%)	Nucleating agent (phr)
X01	85	15	0
X02	85	15	0.4
X03	85	15	1
X04	85	20	0
X05	85	20	0.4
X06	85	20	1

4.3.2 Preparation of Composite Foam Samples

Regarding preparation of non-isotropic foams, sisal fiber/polypropylene composite foams are prepared to be the non-isotropic foam samples. Polypropylene pellets Moplen HP500N from HMC Polymer are mixed with 0 and 20 phr of sisal fibers and maleic

anhydride grafted polypropylene (MA-g-PP) of 0, 2, 5 and 10 wt%. Sisal fiber, polypropylene, and MA-g-PP are mixed in the internal mixture at 190 °C for 10 minutes. Then the mixes are casted by compression molding at mold temperature of 230 °C for 45 minutes. The composite foam samples are produced by physical foaming process using carbon dioxide as the foaming agent at 12 Mpa 165 °C for 2 hours.

Table 4.3 Compositions of sisal fibers reinforced polypropylene composites.

Sample	Sisal fiber (phr)	MA-g-PP (wt%)
Y01	0	0
Y02	20	0
Y03	20	2.0
Y04	20	5.0
Y05	20	10.0

4.3.3 Foaming Apparatus

Foaming apparatus for preparation of the foam samples in Sections 4.3.2 and 4.3.3 consists of CO_2 vessel, high pressure pump, high pressure vessel, silicone oil bath, temperature controller set, propeller, and piping system, as shown in Figure 4.3.

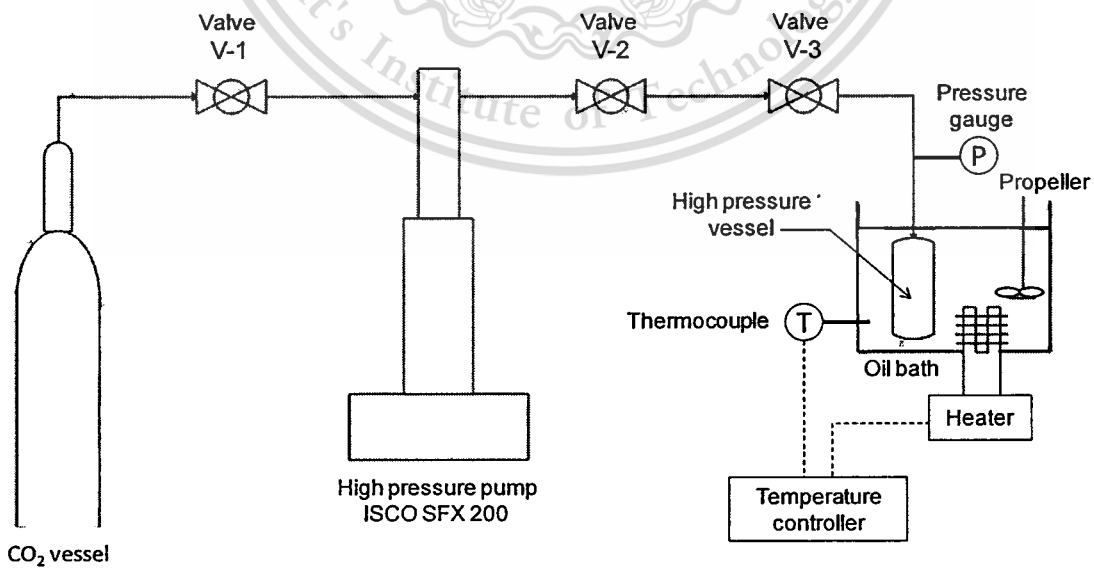

Figure 4.3 Foaming apparatus in preparation of foam samples.

The foaming procedure was explained as follows:

1) Put a polymer/composite sample into the aluminum rack (Figure 4.4).

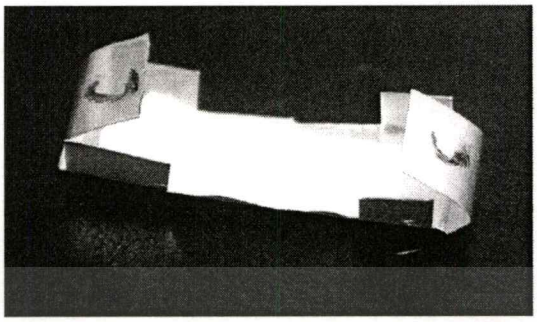

Figure 4.4 Aluminum rack.

2) Open a top end of high pressure vessel (Figure 4.5) and load the aluminum rack into.

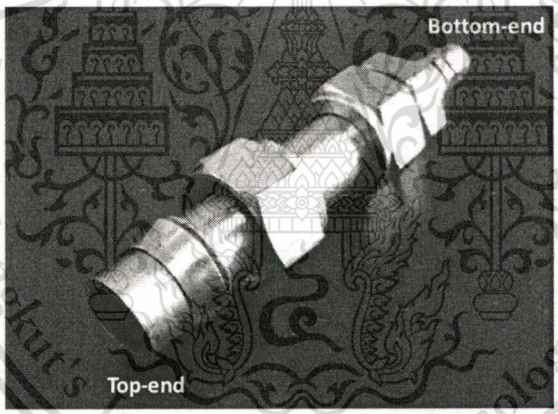

Figure 4.5 High pressure vessel.

3) Cover the high pressure vessel, connect to the valve V-3 piping system as in Figure 4.6, and check for leak test.

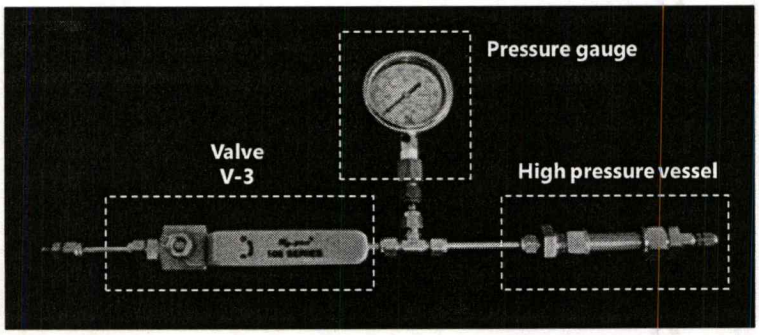

Figure 4.6 Valve V-3 piping system and a foaming high pressure vessel.

4) Connect the valve V-3 piping system to the ISCO SFX 200 high pressure pump (Figure 4.7), as in Figure 4.3.

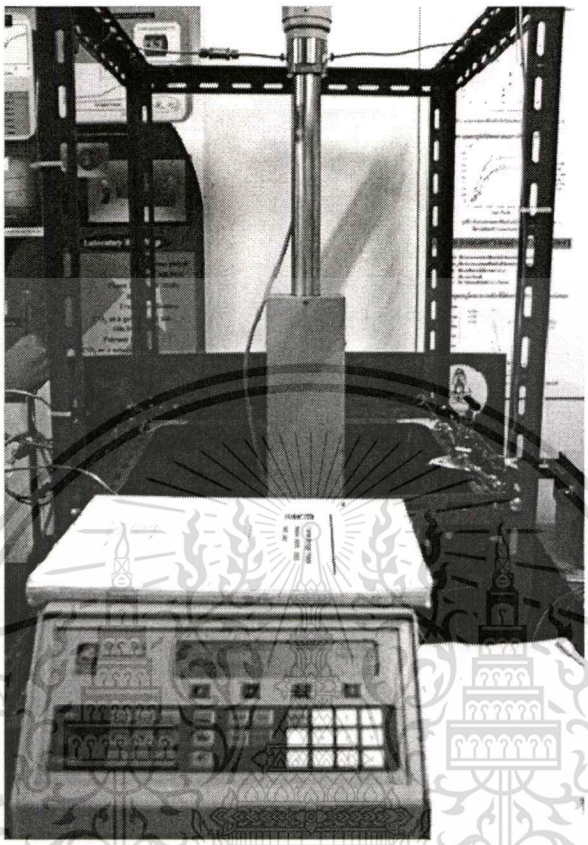

Figure 4.7 ISCO SFX 220 high pressure pump.

5) Provide the temperature-controlled oil bath and propeller as seen in Figure 4.8. Then, program the foaming temperature set point to the temperature controller.

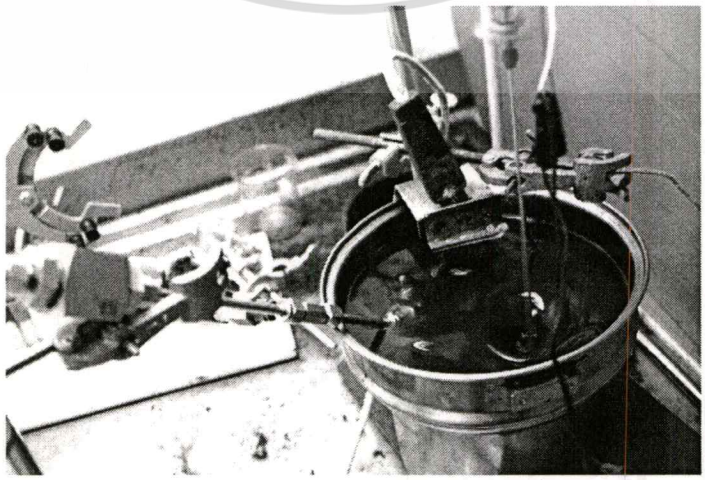

Figure 4.8 High pressure vessel in temperature controlled oil bath.

6) Clear the cavity in the high pressure pump by press RUN button on the high pressure pump controller to compress the piston of the pump until the volume is about 2-3 ml.

7) Feed carbon dioxide from the CO_2 vessel to the high pressure pump: close the valves V-2 and V-3, open the valve V-1, and press the REFILL button until the volume of the pump equals to 250ml, then press STOP button.

8) Compress carbon dioxide gas in the pump to increase pressure: close the valve V-1, press button A to program the set-point pressure and press the ENTER button, then press RUN button. The pump operates until the pressure equaled to the set-point.

9) Open the valves V-2 and V-3 to increase and maintain the pressure of the high pressure vessel.

10) Put the high pressure vessel into the temperature controlled oil bath and start timing.

11) Operate the foaming apparatus system according to scheduled foaming time.

12) Close the valves V-2 and V-3, and then carry off the high pressure vessel from oil bath.

13) Unscrew the joint between valves V-2 and V-3 to separate the piping system of high pressure vessel.

14) Open the valve V-3 to release pressure of the high pressure vessel suddenly to foam the polymer/composite sample.

15) Uncover the top-end of the high pressure vessel and pick out the foam sample.

4.3.4 Methods of Characterization

Final foam samples were cracked with cryogenic cracking in liquid nitrogen. The samples were then observed the morphologies using scanning electron microscope (SEM) to measure average bubble sizes, average cell sizes, and surface cell densities, as explained below.

1) Study of Foam Morphology using Scanning Electron Microscope

Morphological study of a polymeric foam sample is to analysis the cell size and the cell structure of a foam sample from SEM micrograph. A foam sample was prepared by cryogenic cracking in liquid nitrogen, then gold conductive coated with SC 7620 sputter coater as in Figure 4.9, and study foam morphology by using LEO 1455VP scanning electron microscope as in Figure 4.10.

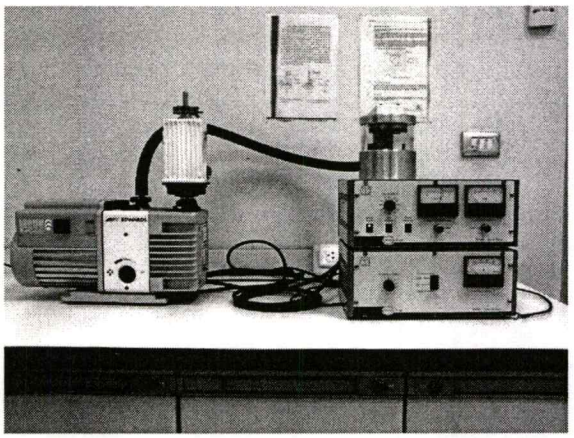

Figure 4.9 SC 7620 sputter coater.

Figure 4.10 LEO 1455VP scanning electron microscope.

2) Estimation of Surface Cell Density using ImageJ

ImageJ is an open-source freeware application, a public domain Java image-processing program, which designed with an open architecture that provides extensibility via Java plug-ins. For example, the surface cell density of a polyethylene foam sample in Figure 4.11 was measured.

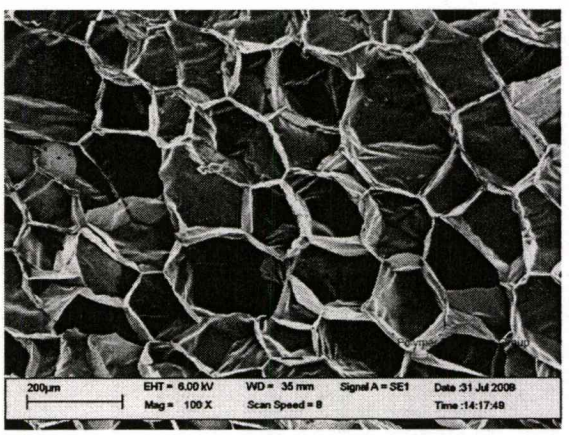

Figure 4.11 Morphology of foam sample from micrograph.

The procedures of the investigation of surface cell density using ImageJ were described as follows:

1) Identify cells of interest and boundary as in Figure 4.12.

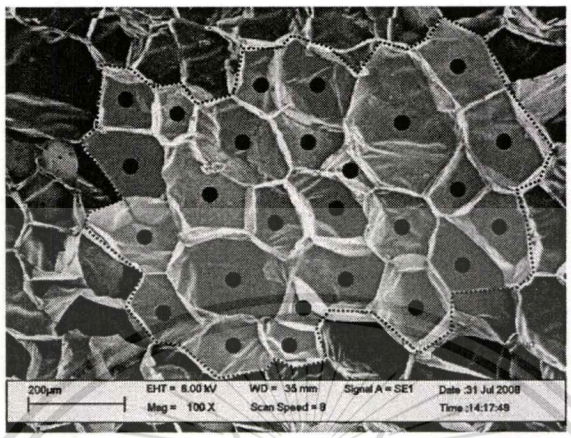

Figure 4.12 Twenty six identified cells of interest (blacked point) and boundary (dashed line).

2) Set scale.

2.1) Use the Straight Line Selections tool, lines the ends of scale bar in micrograph, as in Figure 4.13.

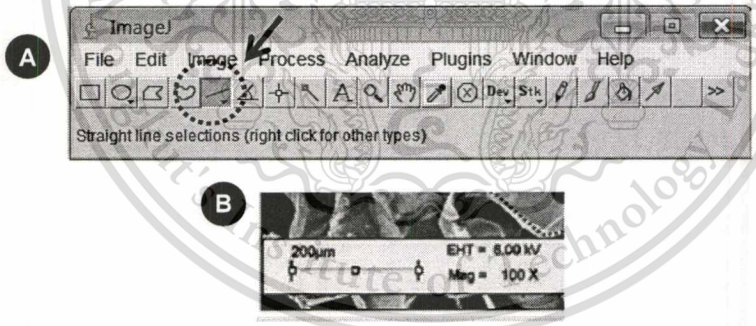

Figure 4.13 (A) Straight Line Selections tool and (B) a scale bar of micrograph.

2.2) Go to menu Analyze, and then select Set Scale, as in Figure 4.14.

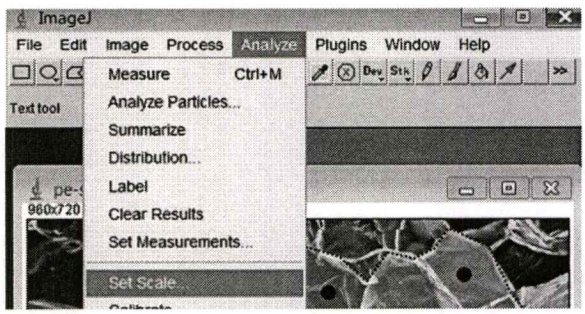

Figure 4.14 Set scale submenu in the analyze menu.

2.3) The Set Scale dialogue displays. Distance in pixels was set automatically with the length of scale bar. Set known distance and unit of length as shown in micrograph (200 μm), as in Figure 4.15, and then click OK.

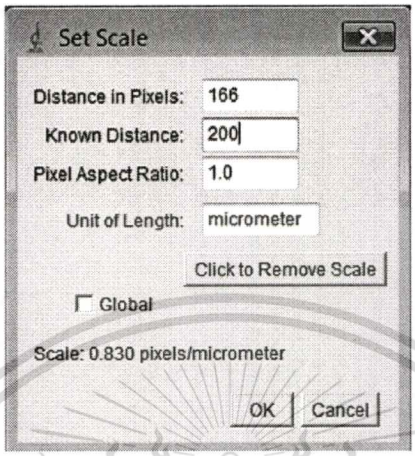

Figure 4.15 Set scale dialogue.

3) Measure the area of boundary.

3.1) Use the polygon selections tool shown in Figure 4.16A, to select boundary of interest for measuring the area of interest, as Figure 4.16B.

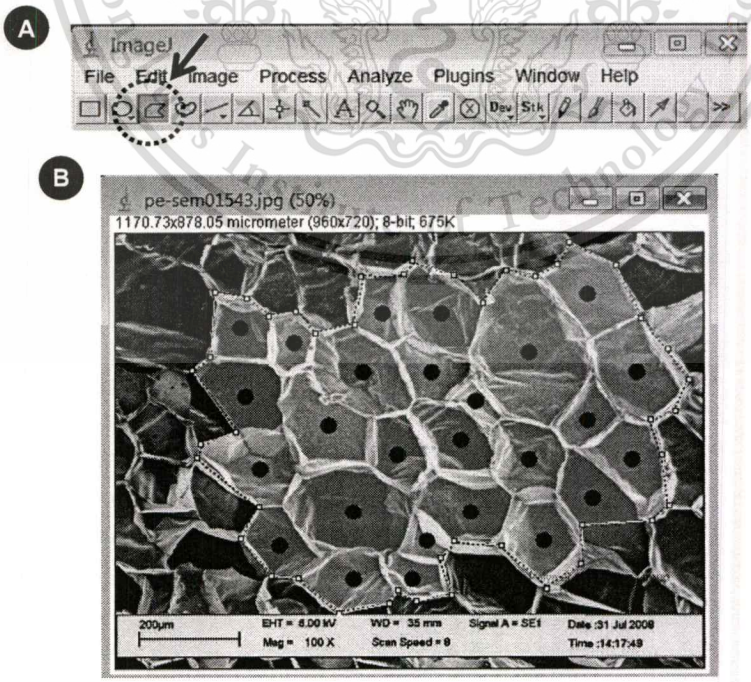

Figure 4.16 (A) Polygon selections tool on toolbar and (B) boundary of the cells of interest.

3.2) Go to menu Analyze, and then select Measure, as in Figure 4.17.

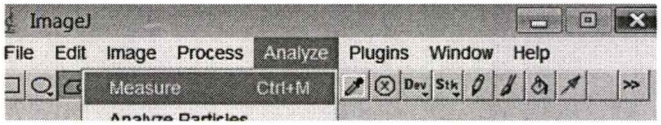

Figure 4.17 Measure submenu in the analyze menu.

3.3) The results dialogue displays as in Figure 4.18 (in unit square of the unit set in set scale step before).

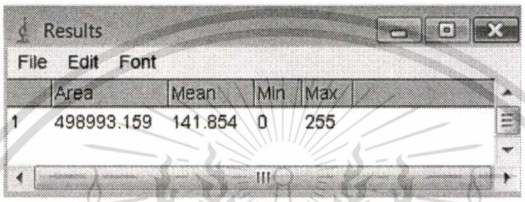

Figure 4.18 Result of measuring area of interest in Results dialogue.

4) Calculate the surface cell density.

Surface cell density of a foam was calculated with the number of identified cells (n) in Figure 4.13 and area of the boundary of interest (A) as shown in the results dialogue in Figure 4.19. The calculation of surface cell density was followed Equation (2.9).

$$N_S = \frac{n}{A} \tag{2.9}$$

For example, the calculation of surface cell density was shown as below.

Number of cells (n) seen in Figure 4.12 = 26 cells

Area of interest (A) seen in Figure 4.18 = 498,993 μm^2

Surface cell density (N_S) = $26/498{,}993$ cell/μm^2

= 5.21×10^{-5} cell/μm^2

$$= \frac{5.21\times10^{-5}\ \text{cell}/\mu m^2 \quad \big| \quad 1\times10^{12}\ \mu m^2}{\qquad\qquad\qquad\quad \big| \quad 1\times10^{4}\ cm^2}$$

= 5.21×10^{3} cell/cm^2

3) Measurement of Bulk Density using Electronic Densimeter

Bulk densities of polymer and polymeric foam samples were measured by using an electronic densimeter MD-200S by A&D co. ltd. with density resolution ±0.001 g/cm^3, as shown

in Figure 4.19. The electronic densimeter applies Archimedes' principle of buoyancy force to investigate density of a sample using water as the reference liquid.

Procedures of measuring bulk density of a sample were described as follows:

(1) Turn on the electronic densimeter before measuring for 10 minutes.

(2) Set zero.

(3) Put the sample on the top of electronic densimeter and then press button A for weighting the sample in atmosphere and save data as shown in Figure 4.19A.

(4) Put a sample in water under the metallic rack as shown in Figure 4.20, and press button A again for weighting in reference liquid water, save data and compute the bulk density.

(5) The bulk density of the sample displays on monitor as seen in Figure 4.19B.

(6) Pick out the sample from electronic densimeter.

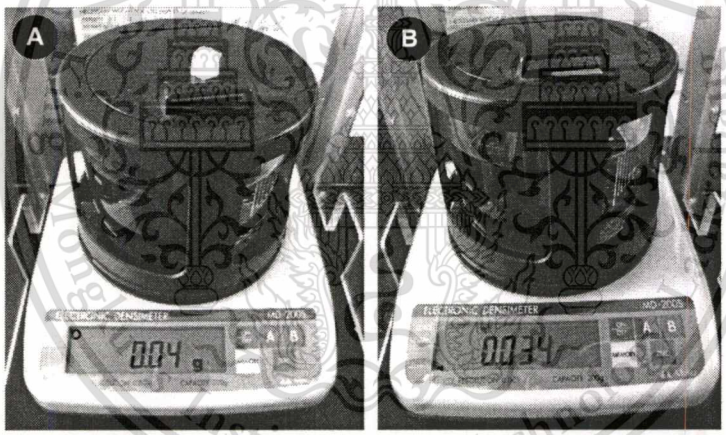

Figure 4.19 Electronic densimeter MD-200S: (A) Weighting sample in atmosphere, and (B) Displayed bulk density of the sample after weighting in water.

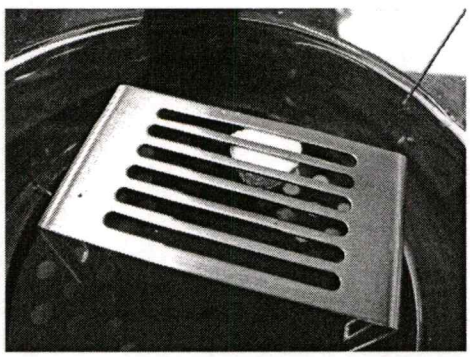

Figure 4.20 A metallic rack for weighting a sample in water.

4.3.5 Method of Analysis

Essential parameters of interest in experiment are expansion ratio, cell size, surface cell density, material balance-based cell density, and isotropic foam index. These parameters are estimated as follows:

1) Expansion ratio

Expansion ratio is measured with assumption that mass of gas less than of polymer relatively by using the ratio of bulk densities of unfoamed polymer and foam, obtained by Equation (2.4).

$$\phi = \frac{\rho_P}{\rho_F} \tag{2.4}$$

2) Average Cell size

Average cell size is measured from micrograph and calculated by using simple average bubble size as seen in Equation (2.8).

$$d = \frac{\sum d_i n_i}{\sum n_i} \tag{2.8}$$

3) Surface cell density

Surface cell density is investigated with the known cell count method, which identifies cells of interest (n) and measures cell cross-sectional windows area of these cells (A), and then calculated by Equation (2.9).

$$N_S = \frac{n}{A} \tag{2.9}$$

4) Material balance-based cell density

Cell density of foam is calculated with material balance based-model, obtained by Equation (1.3).

$$N_F = \frac{\pi d^3}{6}\left(1 - \frac{1}{\phi}\right) \tag{4.3}$$

5) Isotropic Foam Index

Isotropic foam index of a foam is calculated by Equation (3.15).

$$\eta = \log\left(\frac{N_F}{N_F^o}\right) \tag{3.15}$$

Where

$$N_F^o = \varphi_o [N_S]^{\frac{3}{2}} \tag{3.12}$$

Chapter 5

Results and Discussion

5.1 Characterization of Cell Density with Principle of Critical Bubble Lattice

5.1.1 Reliability and Scope of Material Balance-Based Cell Density Estimation using the Critical Bubble Lattice Method

At present, the true cell density of polymeric foams cannot be quantified. The most reliable predictive model is the material balance-based model. Equation (2.20) can be used directly for high density foams. For low density foam, the material balance-based model can be used by modifying it in terms of the critical bubble lattice, as shown in Equation (3.2). The critical bubble concept, as illustrated in Figure 3.5, can be applied to not only high density and low density closed-cell foams, but also open-cell foams by considering them as low density closed-cell foams with a pseudo-wall thickness. Therefore, the material balance-based model with a critical bubble lattice can be applied to all foam morphologies, independent of bubble shape or size by analyzing the cell boundaries.

5.1.2 FCC Lattice as the Maximum Limit of Estimation

The FCC lattice (α=1.415) was considered to be the maximum value for cell density estimation compared with previous experimental data [47-52]. Figure 5.1 illustrates the actual periodic lattice structures of both conventional and microcellular foams; agreement with the model of the foams having typically pentagonal dodecahedral cells packed in an FCC lattice. The good fit of experimental data to the model indicates that the FCC lattice can be applied to these foams, although some of the experimental data falls below the line for the FCC model. The periodic factor α refers to the periodic structure of foams. Because the FCC lattice is the densest packed structure of equally-sized spheres, it is the theoretical upper limit for the estimation of cell density of isotropic foams. Thus, $\alpha \leq 1.414$ is the theoretical limit condition for cell density estimation in Equation (3.3).

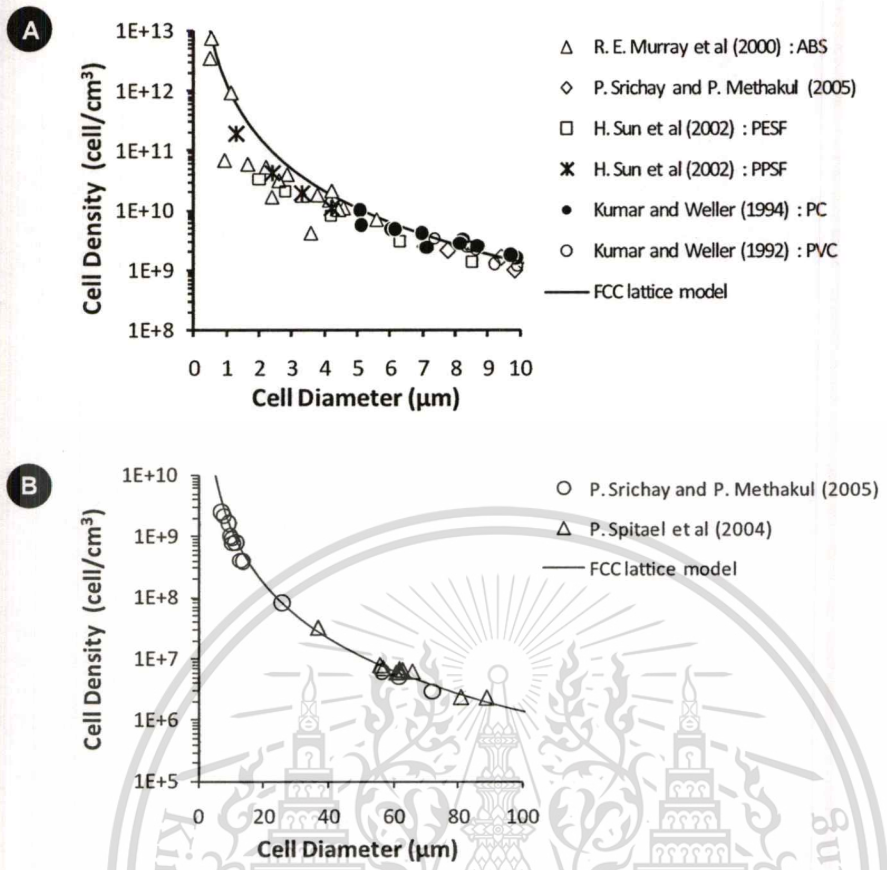

Figure 5.1 Relationship between cell density and average cell size of (A) microcellular foams and (B) conventional foams.

5.1.3 Theoretical Range of Estimation of Cell Density for Isotropic Foam

To investigate the cell density of polymeric foams using Equation (3.10), cell cross-sectional windows must be considered, which may be perfect (κ=1.0746) or non-perfect (κ=2.1354). In the case of perfect cross-sections with pentagonal dodecahedral cells (φ=1.1398) arranged on an FCC lattice, the calculation results in the maximum cell density. Because of uncertainty in cell cross-sectional windows which may either be perfect or non-perfect, the value of apparent factor can fall in the range $1.0746 \leq \kappa \leq 2.1354$ (-). Assuming pentagonal dodecahedral cells on an FCC lattice, calculation result from Equation (3.11) may appear within $0.1453 \leq \varphi \leq 1.1398$ (-), as shown in Figure 4.1. Using the same cell size, the calculated cell density of an FCC lattice with a perfect cross-section window (upper estimation limit) is about ten times greater than the cell density calculated with a non-perfect cross-section window (lower estimation limit).

5.1.4 Effect of Non-Perfect Cross-Section on Cell Density Estimation for Isotropic Microcellular Low Density Foams

The FCC-PF model has the maximum value of the area of hexagonal windows, while the FCC-NPF model has a smaller value of the area of hexagonal windows. The calculated cell densities that ignore this effect are overestimated. Thus, the true cell density should be between the values calculated for the FCC-PF and FCC-NPF models. This hypothesis was investigated by comparing it with the experimental data from previous studies by H. Sun *et al.* [47]. Their foam morphologies are shown in Figure 5.2.

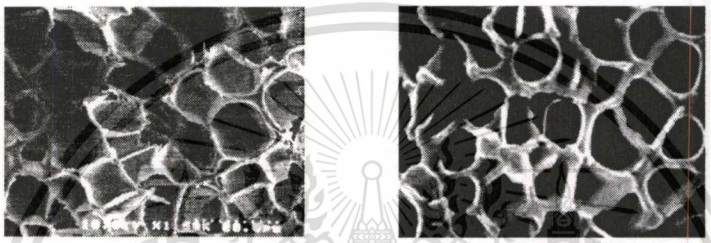

(A) (B)

Figure 5.2 Morphologies of microcellular low density foams: (A) a PES foam and (B) a PPS foam in a study of H. Sun *et al.*(2000) [47].

Most of the experimental data fell in between the two boundaries, as shown in Figure 5.3. The cells were highly isotropic. Only a few experimental data fell outside the range of estimation.

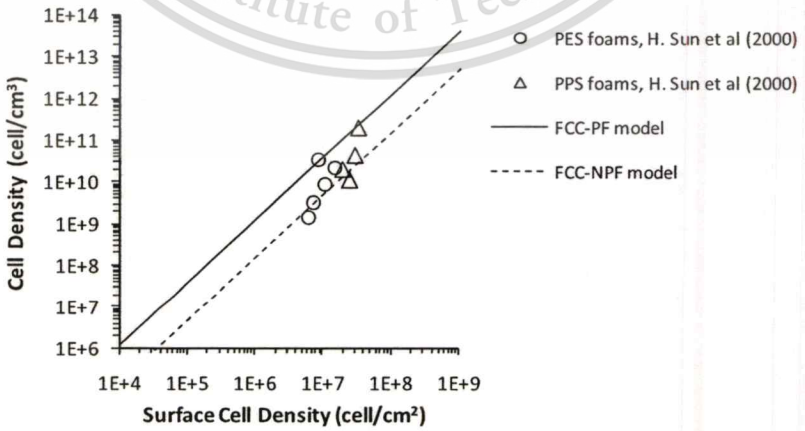

Figure 5.3 Relationship between surface cell density and cell density of microcellular low density foams.

As a result, the percentage average absolute deviation shows that the FCC-NPF model is reasonable to predict the cell density of isotropic low density microcellular foams (AAD=53.2%), which is more reliable than either the conventional model (AAD=405.9%) or the FCC-PF model (AAD=473.5%).

The deviation of cell cross-sectional window area appeared due to the effect of deviation in measuring the surface cell density, as shown in Figure 5.3. Some unobservable cross-sectional area (A*) did not appear. As a result, the true cell density ($N^*_{F,LD}$), as shown in Equation (2.22), was less than that calculated using the FCC lattice with perfect cross-section windows model, as in Equation (5.1).

$$N^*_{F,LD} = 1.1398 \left[\frac{n}{A + A^*}\right]^{\frac{3}{2}} \tag{5.1}$$

In case of conventional low density foams (10-100 μm cell size), polystyrene foams by P.Srichay and P. Methakul [51] were analyzed with the same methods in microcellular forms. The results show that cell densities of the foams were within FCC-PC and FCC-NPF as in Figure 5.4, similar to microcellular low density foams. Some of the experimental data deviated from the assumed range of estimation, which may be caused by non-isotropic effects due to extrusion process.

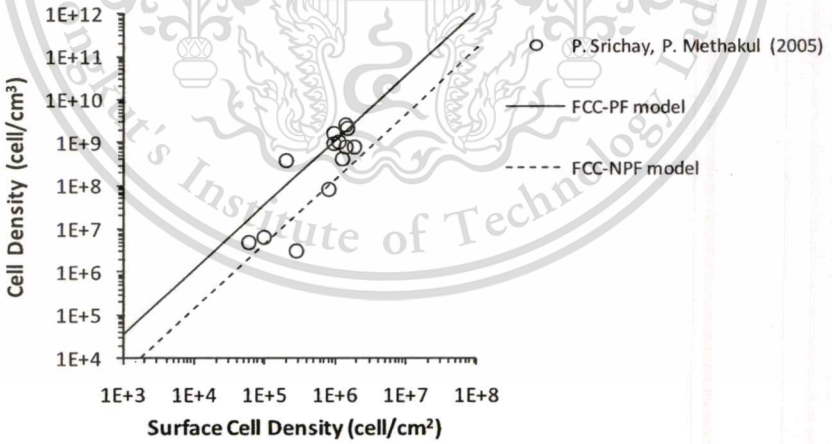

Figure 5.4 Relationship between surface cell density and cell density of conventional low density foams.

5.1.5 Effect of Unobservable Cell Boundaries on Cell Density Estimation for Isotropic Microcellular High Density Foams

For high density foams, a comparison between the cell density from previous experimental data [48-50] (their foam morphologies are shown in Figure 5.5) and the estimation

result of both the conventional and developed models are shown in Figure 5.6. It can be seen that the cell densities measured in all of the previous experiments are higher than those calculated using the FCC-PF model, which is the theoretical maximum.

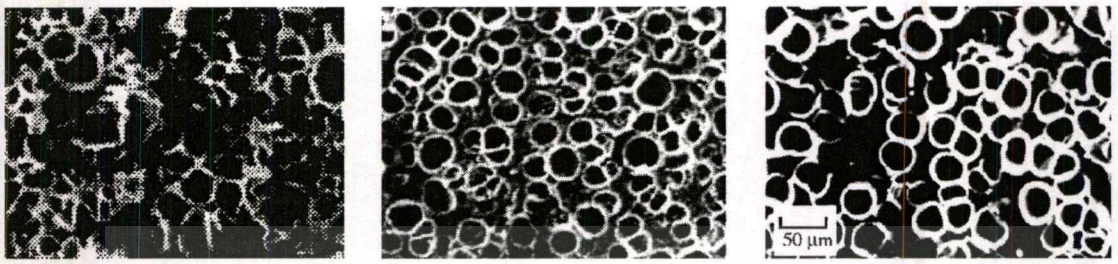

(A) (B) (C)

Figure 5.5 Morphologies of high density foams: (A) ABS foam by E. Murray *et al.* [48], (B) PVC foam by V. Kumar and J. Weller [49] and (C) Polycarbonate foam by V. Kumar and J. Weller [50].

Because of variations in the measured surface cell density due to improper identification of cell window boundaries, it is difficult to identify cell boundaries in high density foam, resulting in a lower apparent cell count than the true value. Some unobservable cells (n*) did not appear in the area of interest on a micrograph, and therefore the cell count is lower than the true value (n+n*), the surface cell density is estimated too low, and the estimated cell density (N_F) is less than the true cell density ($N^*_{F,HD}$), as seen in Equation (5.2).

$$N^*_{F,HD} = 1.1398\left[\frac{n+n^*}{A}\right]^{\frac{3}{2}} \tag{5.2}$$

Thus, the true cell density should be greater than the calculated result using the FCC-PF model ($N_F < N_F^*$).

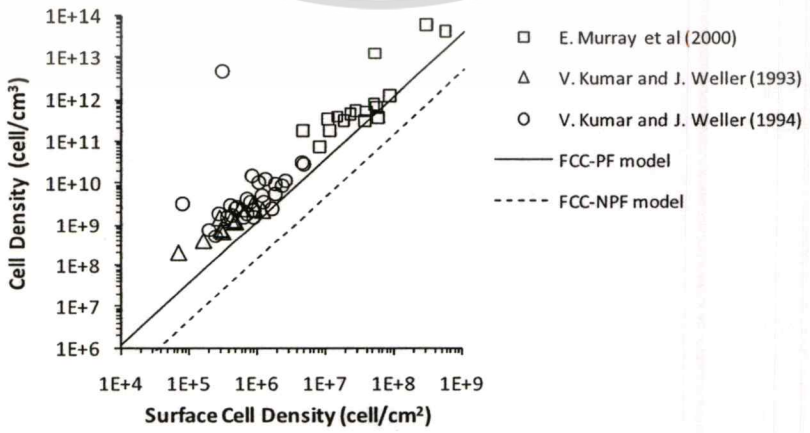

Figure 5.6 Relationship between surface density and cell density of microcellular high density foams.

In Figure 5.6, a comparison of the conventional and the two newly developed models indicate that the FCC-PF model (AAD=68.8%) gives the lowest deviation from the experimental data, while the conventional model (AAD=72.0%) and the FCC-NPF model (AAD=95.8%) deviate more from the experimental data. Therefore, the FCC-PF model appropriately predicts the cell density of an isotropic high density foam.

Furthermore, conventional high density polypropylene foams by P. Spitael and C. Macosko [52] were analyzed with the same methods in microcellular high density foams. As a result in Figure 5.7, material balance-based cell densities as true cell densities of foams were greater than the FCC-PF model, similarly to microcellular foams. Their foam morphologies are in Figure 5.8.

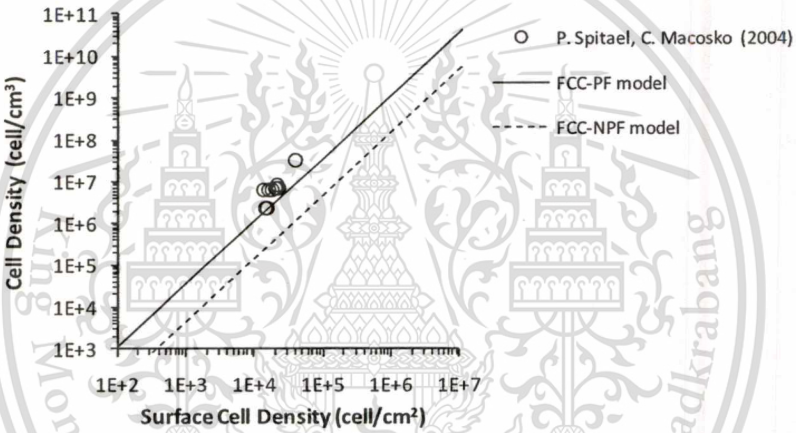

Figure 5.7 Relationship between surface density and cell density of conventional high density foams.

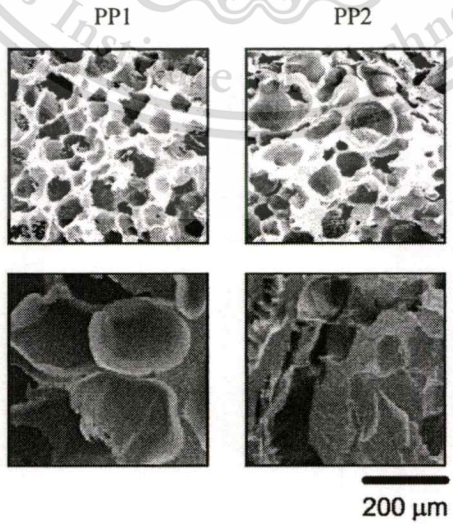

Figure 5.8 Morphology of a conventional high density P foams by P. Spitael and C. W. Macosko (2004) [52]. Top row: 1-mm-diameter die, 10-mm land length. Bottom row: 2-mm-diameter die, 10-mm land length.

5.2 Characterization of Isotropic Foam Behavior with Isotropic Foam Index

5.2.1 Standard Isotropic Factor

In practice, the apparent isotropic factor φ can be derived from regression of the graph of surface cell density versus cell density. In chapter 4, isotropic foam index is introduced and calculated using Equation (3.15). The values of the isotropic factor for both spherical and polyhedral bubbles are discussed. Isotropic high density foams are found to be in a good correlation with the FCC-PF model, and the standard isotropic factor ($\varphi_{o,HD}$) is 1.1398. On the other hand, the FCC-NPF model appropriately predicts the cell density of the isotropic low density foams, and the standard isotropic factor ($\varphi_{o,LD}$) is 0.1453.

5.2.2 Testing of Isotropic Foam Behavior – Investigation of the Isotropic Foam Index

In Figure 4.1, the plot of cell density and surface cell density is a very useful tool to determine whether the foam in question is isotropic or non-isotropic, or how it deviates from isotropic foams. The isotropic foam index (φ) has been introduced to describe this behavior. Isotropic foam index was evaluated by Equation (3.15) and depended on the standard isotropic cell density (N_F^o) from Equation (3.12) and the true cell density (N_F), which is the material balance-based cell density. In the previous section, the standard isotropic factor of high density foam is found to be 1.1398, and isotropic microcellular foam is found to deviate from the FCC-PF model. The range of isotropic behavior between the model and the experiment is calculated. The result indicates that isotropic low density foams behave in a manner between the FCC-PF and FCC-NPF models, and the isotropic foam index of low density foams should be within the range of 0 and 0.895.

5.3 Validation of Models

5.3.1 Polyethylene Foam Samples

Polyethylene foams were prepared. Their foam morphologies were shown in Figure 5.9. All of the foam morphologies are mono-size polyhedral foams, the cell sizes were in range 23.8 – 56.1 μm, volume expansion ratios were in range 2.67 – 7.61 g/cm^3, and surface cell densities 6.08×10^4 – 1.78×10^5 cell/cm^3. Foam properties were shown in Table 5.1.

Table 5.1 Properties of polyethylene foam samples foamed at 150°C 12 MPa for 2 hours.

Sample	Polymer-A (wt%)	Polymer-B (wt%)	Nucleating agent (phr)	Density of resin (g/cm^3)	Density of foam (g/cm^3)	Expansion ratio (-)	Cell size (μm)	Surface density ($cell/cm^3$)
X01	85	15	0	0.948	0.256	3.70	23.8	1.78E+05
X02	85	15	0.4	0.944	0.124	7.61	56.1	6.08E+04
X03	85	15	1	0.936	0.200	4.68	37.0	1.39E+05
X04	80	20	0	0.946	0.298	3.17	32.6	1.13E+05
X05	80	20	0.4	0.943	0.210	4.49	37.3	1.37E+05
X06	80	20	1	0.936	0.351	2.67	45.5	9.24E+04

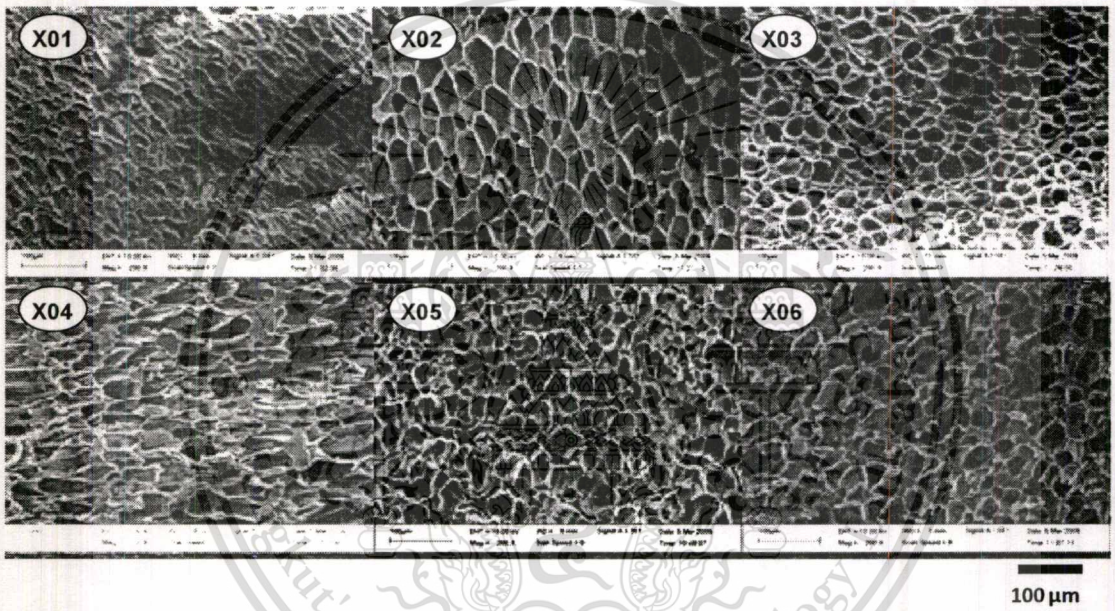

Figure 5.9 Foam morphologies of polyethylene foam samples:
(A) X01, (B) X02, (C) X03, (D) X04, (E) X05, and (F) X06

Foaming apparatus produce a foam sample with free-rise process to make isotropic foam. Cell cross-section shows that Sample X02, X03, X05, and X06 were symmetry in bubble shape. Sample X01 and X03 were non-symmetry in shape and could be non-isotropic.

Figure 5.10 illustrates the plots of material balance-based cell density versus cell size to compare the developed model. The experimental cell densities were near to the FCC lattice model, which is the theoretical maximum limit of the estimation of cell density. This is in agreement with the discussion in section 5.1.1.

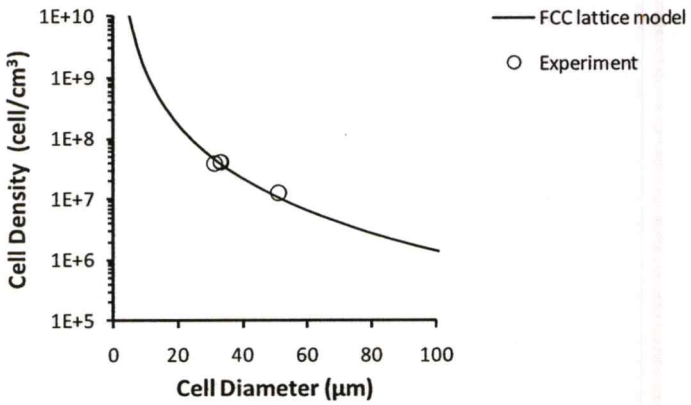

Figure 5.10 Relationship between cell density and cell diameter of polyethylene foam samples.

Figure 5.11 illustrates the relationship between cell density and surface cell density of polypropylene foam samples. The experimental cell densities, which were estimated by the material balance-based model, were between the values those calculated by the FCC-PF and FCC-NPF models. For isotropic foam, i.e., samples X02, X03, X5, and X06. Most of the experimental data fell in between the two boundaries, in agreement with the discussion in section 5.1.2.

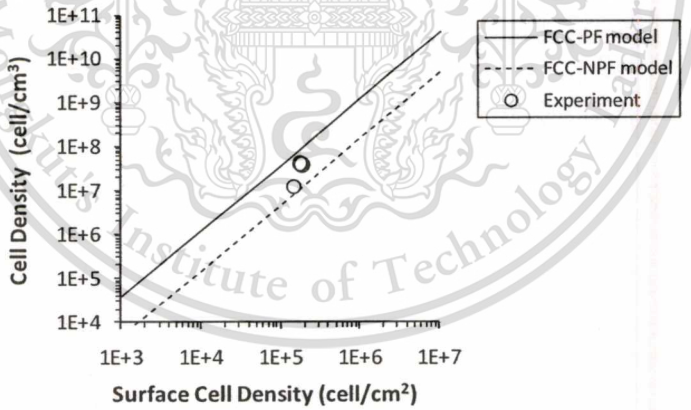

Figure 5.11 Relationship between cell density and surface cell density of the foam samples: X02, X03, X05, and X06.

For sample X01 and X03, the relationship between cell density and surface cell density of non-isotropic foam samples, some of the experimental cell densities deviated from the range of estimation as seen in Figure 5.12.

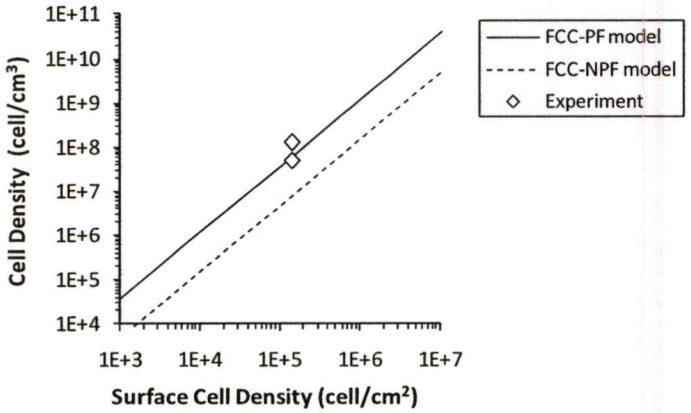

Figure 5.12 Relationship between cell density and surface cell density of the foam samples: X01 and X03.

5.3.2 Composite Foam Samples

The experiment for testing of composite foam samples in section 4.3.2 was investigated. Morphologies of sisal fiber-reinforced polypropylene composite foams are shown in Figure 5.13. The non-isotropic foams are caused by non-uniform orientation of sisal fiber and cross-linking effect of MA-g-PP.

1) Effect of Sisal Fiber on Foam Morphology and Isotropic Properties

In Table 5.2, expansion ratio of PP mixed with sisal fiber was less than neat PP about 4 times cause by foam microstructure due to the existence of sisal fiber. Sisal fiber affects mono-size distribution. Expansion ratio was decreased with decreasing of cell size [46]. Furthermore, when compared with the bulk density of unfoamed PP resin, the bulk density of PP mixed with 20 phr of sisal fiber was greater than neat PP about 4%. Because bulk density of sisal fiber of 1.26 g/cm^3[53] is greater than that of PP resin, effect of increasing of bulk density of composite can be expected as the sisal fiber increases in amount.

Table 5.2 Properties of sisal/PP composite foam samples foamed at 165°C 12 MPa for 2 hours.

Sample	Sisal fiber (phr)	MA-g-PP (%)	Density of resin (g/cm^3)	Density of foam (g/cm^3)	Expansion ratio (-)	Cell size (μm)	Wall thickness (μm)	Surface density (cell/cm^3)	Secondary cell size (μm)	Secondary Surface density (cell/cm^3)
Y01	0	0	0.904	0.196	4.52	4.3	1.2	1.92E+10	77.4	3.84E+06
Y02	20	0	0.955	0.813	1.17	6.2	1.7	9.36E+08	-	-
Y03	20	2	0.934	0.541	1.73	17.1	2.5	1.83E+08	-	-
Y04	20	5	0.929	0.580	1.60	18.5	2.0	2.83E+08	185.1	3.40E+04
Y05	20	10.0	0.947	0.578	1.64	28.5	6.5	4.08E+07	168.9	7.70E+04

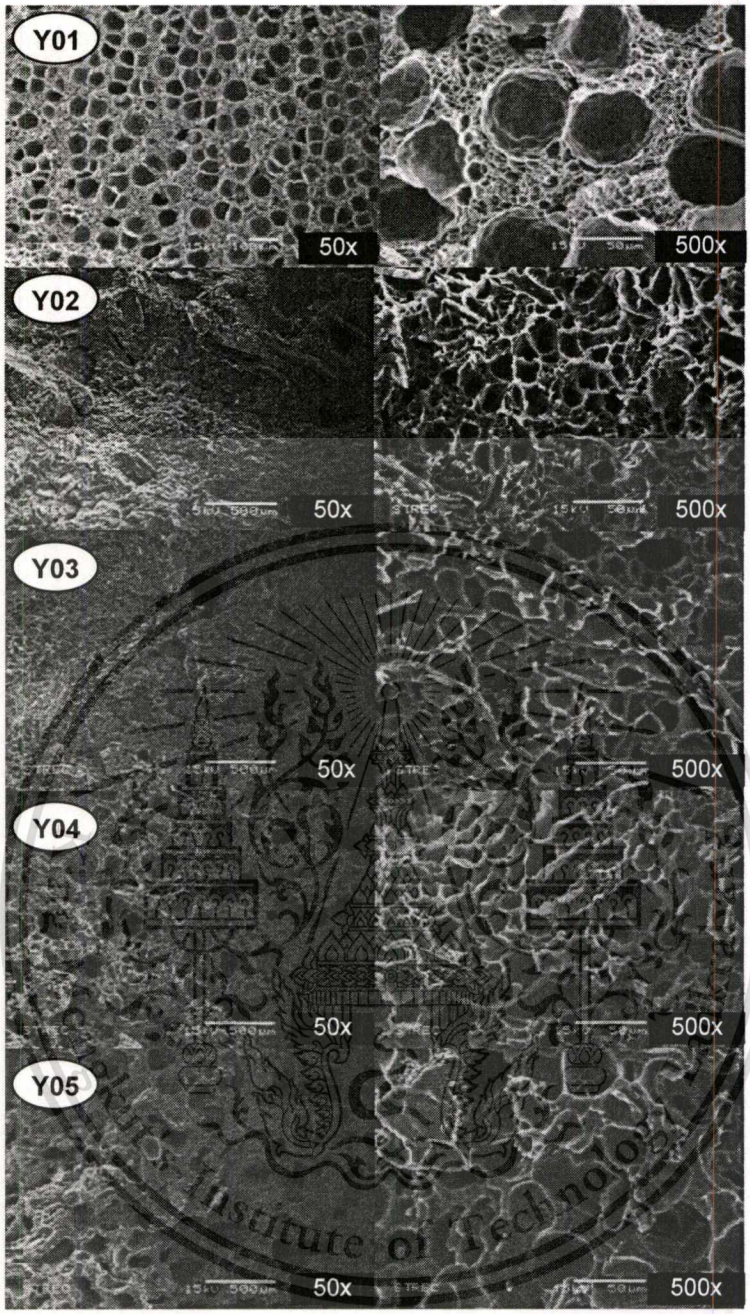

Figure 5.13 Morphologies of foam samples: (A) neat PP, (B) 20phr sisal fiber/PP composite foams, (C) 98%PP 2%MA-g-PP, (D) 95% PP 5% MA-g-PP and (E) 90% PP 10%MA-g-PP, foaming at 165 °C, 12 MPa for 2 hours.

In morphological study of composite foam samples, the results showed that cell structure of neat PP was bimodal with average primary cell size of 4.3 μm and average secondary cell size of 77.4 μm, as shown in Figure 5.13A. On the other hand, cell structure of PP mixed with 20 phr sisal fiber composite foam was uniformly mono-size with average cell size of 6.2 μm, which was closed to the average primary cell size of neat PP foam, as shown in Figure 5.13B.

Mixture of sisal fiber in PP resin may increases crystallinity of sisal fiber-dispersed PP resin because sisal fiber is formed from cellulose microfiber. Adhesive force between the fiber and PP resin causes the viscosity of resin increases [54]. Moreover, celluloses at surface of the fiber polymer behave as nucleating agent. For these reasons, nucleation and expansion of gas bubbles are uniform, bimodal structure did not appear.

2) Effect of MA-g-PP on Foam Morphology and Isotropic Properties

Table 5.2 shows that MA-g-PP affects the volume expansion ratios increase about 1.4 times. All of the sisal fiber/PP mixed with MA-g-PP composite foams have volume expansion ratios about 1.6 (-), while sisal fiber/PP composite without MA-g-PP has 1.17 (-). MA-g-PP was used as a compatibilizer between the reinforced sisal fiber and PP resin. Mixing MA-g-PP into sisal fibers/PP resins causes the viscosity of the sisal fiber/PP resin to increase and the expansibility of gas bubbles to decrease [55]. In addition, cell size and population density of secondary bimodal bubbles at 10 %MA-g-PP are greater than of that 5%. These may be caused by cell collapsing effect. That is, popular density and cell size of secondary bimodal bubbles increase with increasing amount of MA-g-PP. Some gas bubbles are larger than no-collapse-expanse gas bubbles, and bimodal foam structure can appear, as in Figures 5.13B and 5.14C at MA-g-PP greater than 5%. Gas bubbles that their pressures are less than surface tension of the resin can collapse; the gas inside those can diffuse to their neighbor bubbles. Moreover, because solubility of CO_2 dissolved in MA-g-PP is less than in PP, solubility of CO_2 in bulk resin decrease. From this reason, Increasing of amount of MA-g-PP causes nucleus density of nuclei in the resin to decrease, average distant between nuclei and average wall thickness to increase.

In conclusion, mixture of sisal fiber, polypropylene and MA-g-PP in preparations of composite foams affects to uniformity of morphologies of foams, with mono-distributed microstructure. Bulk density, expansion ratio, cell size and wall thickness increase with increasing of MA-g-PP. Finally, sisal fiber and MA-g-PP cause deviation of isotropic properties in composite foams.

3) Test of Isotropic Foam Property

The plot of cell density at cell size, Figure 5.14 shows that the experimental cell densities were below those from the FCC lattice model, which are the theoretical maximum limit of the estimation of cell density.

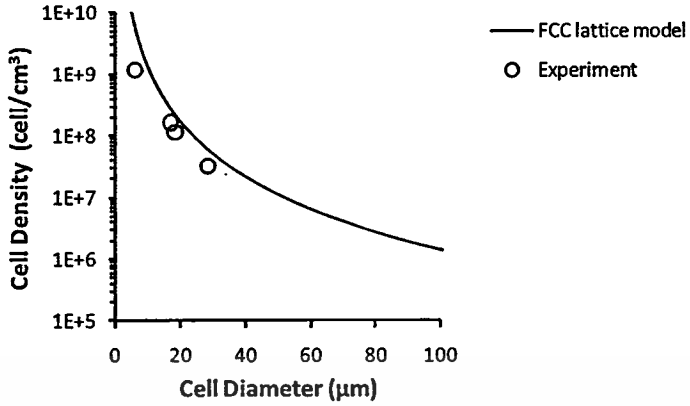

Figure 5.14 Relationship between cell density and cell diameter of composite foam samples.

Figure 5.15 illustrates the relationship between cell density and surface cell density of isotropic foam samples. Some of the experimental data deviated from the range of estimation because of non-isotropic effects caused by sisal fibers and MA-g-PP.

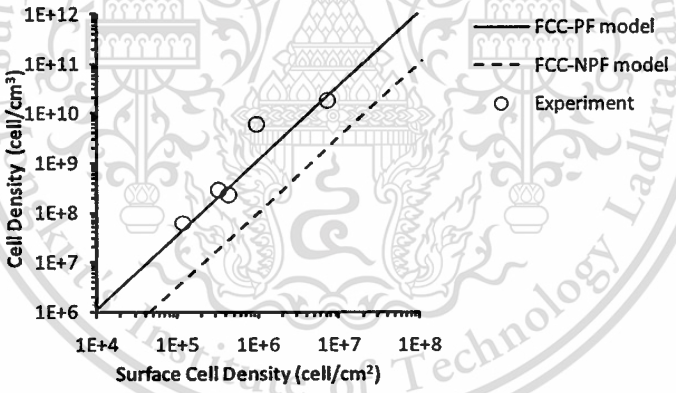

Figure 5.15 Relationship between cell density and surface density of composite foam samples.

In conclusion, the results from the testing for isotropic and non-isotropic foam samples show that the range of estimation between FCC-PF and FCC-NPF models can be used to characterize the isotropic foam behavior of low density foams.

Chapter 6

Summary, Conclusions, and Suggestions

6.1 Summary of Contributions

1. The newly-developed critical bubble model is used to analyze cell structure for the estimating cell density with uniform or non-uniform distribution of gas bubbles. Similarities between critical bubble lattice and atomic packed structure are considered. The equation of cell density estimation for the atomic packing model is applied to the periodic foam structure model. The cell density of foam is equal to cell density of the similarly atomic packed structure, which is independent to shape and size of the gas bubbles inside the cells, or foaming process.

2. The concept of bubble rearrangement is used to rearrange random dispersed gas bubbles into a periodic structure, for applying perfect cell cross-section model to the estimation of cell density of high density foam.

3. Periodic pattern of foam microstructure can be indicated with periodic factor (α). Cell cross-sectional windows appear uncertainly within perfect and non-perfect can be indicated with apparent factor (κ). The general form of the mathematical relationship between cell density and surface cell density can be demonstrated by using isotropic factor (φ). The isotropic factor also exhibits as the correcting factor for the conventional cell density model.

4. The FCC lattice with perfect cell cross-section model (FCC-PF: α=1.4142, κ=1.0746, φ=1.1398) and FCC lattice with non-perfect cell cross-section model (FCC-NPF: α=1.4142, κ=2.1354, φ=0.1453) were developed to study the effect of cell cross-sections on cell density estimation of pentagonal dodecahedral foams.

5. Standard isotropic foam refers to the perfect isotropic foam structure. Standard isotropic cell density (N_F°) is the cell density of the standard isotropic foams. Standard isotropic factor (φ_o) is used for estimation of isotropic foam using surface cell density from cell cross-section as a parameter. The value of standard isotropic factor depends on cell structure or appeared foam morphology from micrograph. The isotropic foam index (η) is defined to indicate deviation from the isotropic foam behavior, given as the logarithm of the ratio of apparent isotropic factor and standard isotropic factor. In practice, the isotropic foam index can be evaluated by taking logarithm of the ratio of the cell density and standard isotropic cell density.

6.2 Conclusions

1. The cell density of an isotropic polymeric closed cell foams is possibly within the range of those predicted by the FCC-PF and FCC-NPF models ($0.1453<\varphi<1.1398$) due to uncertainty of the apparent cell cross-sections of pentagonal dodecahedral cells.

2. The FCC-PF model was appropriate to predict the cell density of an isotropic microcellular high density foam with reliability of 68.8%AAD, which is more reliable than either the conventional model (AAD=72.0%) or the FCC-NPF model (AAD=95.8%).

3. The FCC-NPF model was appropriate to predict the cell density of an isotropic microcellular low density foam with reliability of 53.2 %AAD, which is more reliable than either the conventional model (AAD=405.9%) or the FCC-PF model (AAD=473.5%).

4. The standard isotropic factors of high density and low density foams are 1.1398 and 0.1453, respectively.

5. The range of estimation between FCC-PF and FCC-NPF models can be used to characterize the isotropic foam behavior of polymeric foams. The isotropic foam index of an isotropic low density foam is possibly within the range of 0 and 0.895.

6.3 Suggestions

Future researches could be:

1. The validation for open-cell foams should be conducted.

2. The other cell structure such as tetrakaidecahedron cells with BCC lattice, which is one of typically cell structures of open-cell foams, should be studied.

3. More accurate method of measuring the true cell density of low density foams should be developed and applied.

4. Criteria and ranges of isotropic foam index for acceptable bounds of deviation from isotropic foam should be studied.

References

[1] V. Shulmeister, M. W. D. Van der Burg, E. Van der Giessen and R. Marissen. "A numerical study of large deformations of low-density elastomeric open-cell foams." **Mechanics of Materials**, vol. 30, pp. 125-140, 1998.

[2] K. W. Suh, C. B. Park, M. J. Maurer, M. H. Tusim, R. D. Genova, R. Broos and P.S. Daniel. "Lightweight cellular plastics." **Advanced Materials**, vol. 12, pp. 1779-1789, 2000.

[3] V. Kumar. "Microcellular polymers: Novel materials for the 21st century." **Cellular Polymer**, vol. 12, pp. 207-223, 1993.

[4] D. L. Tomasko, H. Li, D. Liu and X. Han. "A review of CO2 applications in the processing of polymers." **Industrial & Engineering Chemistry Research**, vol. 42, pp. 6431-6456, 2003.

[5] D. I. Collias and D. G. Baird. "Impact toughening of polycarbonate by microcellular foaming." **Polymer**, vol. 35, pp. 3978-3983, 1994.

[6] B. Krause, H.J.P. Sijbesma, P. Münüklü, N.F.A. van der Vegt and M. Wessling. "Bicontinuous nanoporous polymers by carbon dioxide foaming." **Macromolecules**, vol. 34, pp. 8792-8801, 2001.

[7] S. Doroudiani, C.B. Park and M.T. Kortschot. "Effect of the crystallinity and morphology on the microcellular foam structure of semicrystalline polymers." **Polymer Engineering and Science**, vol. 36, pp. 2645-2662, 1996.

[8] M. Yuan, L.-S. Turng, S. Gong, D. Caulfield, C. Hunt and R. Spindler. "Study of injection molded microcellular polyamide-6 nanocomposites." **Polymer Engineering and Science**, Vol. 44, pp. 674-686, 2004.

[9] R. Gosselin and D. Rodrigue. "Cell morphology analysis of high density polymer foams." **Polymer Testing**, vol. 24, pp. 1027-1035, 2005.

[10] ASTM International. **ASTM D 1622-08: Standard test method for apparent density of rigid cellular plastics.** 2008.

[11] International Organization for Standardization. **ISO 845:2006 – Cellular plastics and rubbers – determination of apparent density.** 2006.

[12] M. Peleg. "Mechanical properties of dry cellular solid foods." **Food Science and Technology International**, vol. 3. pp. 227-240, 1997.

[13] W. Zhai, J. Yu , L. Wu , W. Ma and J. He. "Heterogeneous nucleation uniformizing cell size distribution in microcellular nanocomposites foams." **Polymer,** vol. 47, pp. 7580-7589, 2006.

[14] E. Herrera Tejeda, C. Zepeda Sahagun, R. Gonzalez-Nunez and D. Rodrigue. "Morphology and mechanical properties of foamed polyethylene/polypropylene blends." **Journal of Cellular Plastics**, vol. 41, pp. 417-435, 2005.

[15] J. Xu and L. Kishbaugh. "Simple modeling of the mechanical properties with part weight reduction for microcellular foam plastics" **Journal of Cellular Plastics**, vol. 39, pp. 29-47, 2003.

[16] Lee S. T. **Polymeric foams : technology and science of polymeric foams.** Florida : Tavlor and Francis Group. 1956.

[17] Sue J. W. **"Effect of microstructure of closed cell foam on strength and effective stiffness"** Doctoral dissertion, Material Science and Engineering, Texas A&M University. 2006.

[18] V. Kumar and J. E. Weller. "Production of microcellular polycarbonate using carbon dioxide for bubble nucleation." **ASME Journal of Engineering for Industry,** vol. 116, pp. 413-420, 1994.

[19] Lee S. T. and Ramesh N. S. **Polymeric foams : mechanisms and materials**, Florida : CRC Press. 2004.

[20] Z.-M. Xu, X-L Jiang, T. Liu, G.-H. Hu, L. Zhao, Z.-N. Zhu and W.-K. Yuan. "Foaming of polypropylene with supercritical carbon dioxide." **Journal of Supercritical Fluids**, vol. 41, pp. 299-310, 2007.

[21] D. L. Tomasko, A. Burley, L. Feng, S.-K. Yeh, K. Miyazono, S. Nirmal-Kumar, I. Kusaka and K. Koelling. "Development of CO_2 for polymer foam applications." **Journal of Supercritical Fluids**, vol. 47, pp. 493-499, 2009.

[22] Senses N. **"Foam Structures: A comparative structural efficiency analysis based on the building case Watercube."** M.Sc. Thesis, Building Science & Technology, Vienna Technological University. 2007.

[23] Wikipedia. "Polyhedron" [Online]. Available : http://en.wikipedia.org/wiki/Polyhedron. 2010

[24] W. Jang, A. Kraynik and S. Kyriakides. "On the microstructure of open-cell foams and its effect on elastic properties." **International Journal of Solids and Structures,** vol. 45, pp. 1845-1875, 2008.

[25] A. Fazekas, R. Dendievel, L. Salvo and Y. Brechet. "Effect of microstructural topology upon the stiffness and strength of 2D cellular structures." **International Journal of Mechanical Sciences,** vol. 44, pp. 2047-2066, 2002.

[26] S. Hilgenfeldt, A. M. Kraynik, D. A. Reinelt, and J. M. Sullivan. "The structure of foam cells: isotropic plateau polyhedral." **Europhysics Letters,** vol. 67, pp. 484-490, 2004.

[27] S. G. Kim, S. N. Leung, C. B. Park and M. Sain. "Replacement of cross-linked PP foams and solid TPO products with recyclable TPO foams." **The 6th International Conference on Foam Processing and Technology, Society of Plastics Engineers,** 2008.

[28] Wikipedia. **"X-ray computed tomography"** [Online]. Available : http://en.wikipedia.org/wiki/X-ray_computed_tomography. 2010.

[29] Wikipedia. **"X-ray microtomography"** [Online]. Available : http://en.wikipedia.org/wiki/X-ray_microtomography. 2010.

[30] M. Montminy, A. Tannenbaum and C. Macosko. "The 3D structure of real polymer foams." **Journal of Colloid and Interface Science,** vol. 280, pp. 202-211, 2004.

[31] S. Youssef, E. Maire and R.Gaertner. "Finite element modelling of the actual structure of cellular materials determined by X-ray tomography." **Acta Materialia,** vol. 53, pp. 719-730, 2005.

[32] E. Maire, A. Fazekas, L. Salvo, R. Dendievel, S. Youssef, P. Cloetens, and J. M. Letang. "X-ray tomography applied to the characterization of cellular materials: Related finite element modeling problems." **Composites Science and Technology,** vol. 63, pp. 2431-2443, 2003.

[33] D.L. Sahagian and A.A. Proussevitch. "3D particle size distributions from 2D observations: stereology for natural applications." **Journal of Volcano Geothermal Research,** vol. 84, pp. 173-196, 1998.

[34] S. B. Biner. "Thermo-elastic analysis of functionally graded materials using Voronoi elements." **Materials Science and Engineering A,** vol. 315, pp. 136-146, 2001.

[35] S. Hutzler, J. Barry, P. Grasland-Mongrain, D. Smyth and D. Weaire. "Ordered packings of bubbles in columns of square cross-section." **Colloids and Surfaces A: Physicochemical and Engineering Aspects**, vol. 344, pp. 37-41, 2009.

[36] D. S. Kim, Y. C. Chung, S. Seo, S. P. Kim and C. M. Kim. "Crystal structure extraction in materials using Euclidean Voronoi diagram and angular distributions among atoms." **Journal of Ceramic Processing Research**, vol. 6, no. 1, pp. 63-67, 2004.

[37] V. A. Luchnikov, M. L. Gavrilova, N. N. Medvedev and V. P. Voloshin. "The Voronoi – Delaunay approach for the free volume analysis of a packing of balls in a cylindrical container." **Future Generation Computer Systems**, vol. 18, pp. 673-679, 2002.

[38] L. J. M. Jacobs, K. C. H. Danen, M. F. Kemmere and J. T. F. Keurentjes. "Quantitative morphology analysis of polymers foamed with supercritical carbon dioxide using Voronoi diagrams." **Computational Materials Science**, vol. 38, pp. 751-758, 2007.

[39] K. M. Lewis , I. Kijak , K. B. Reuter and J. B. Szabat. "An image analysis method for cell-size and cell-size distribution measurement in rigid foams." **Journal of Cellular Plastics**, vol. 32, no. 3, pp. 235-259, 1996.

[40] T. T. Huu, M. Lacroix, C. P. Huu, D. Schweich and D. Edouard. "Towards a more realistic modeling of solid foam: Use of the pentagonal dodecahedron geometry." **Chemical Engineering Science**, vol. 64, pp. 5131-5142, 2009.

[41] C. Pozrikidis. "Expansion of a two-dimensional foam." **Engineering Analysis with Boundary Elements**, vol. 26, pp. 495-504, 2002.

[42] K. Li, X. L. Gao, and G. Subhash. "Effects of cell shape and strut cross-sectional area variations on the elastic properties of three-dimensional open-cell foams." **Journal of the Mechanics and Physics of Solids**, vol. 54, pp. 783-806, 2006.

[43] S. L. Evaritt, O. G. Harlen and H. J. Wilson. "Bubble growth in a two-dimensional viscoelastic foam." **Journal of Non-Newtonian Fluid Mechanics**, vol. 137, pp. 46-59, 2006.

[44] Callister, W. D. **Material science and engineering: an introduction, 7th edition.** New York: Wiley & Sons. 2006.

[45] Ribeiro-Ayeh S. **"Finite element modelling of the mechanics of solid foam materials."** Ph.D. Thesis, Aeronautical and Vehicle Engineering, KTH Royal Institute of Technology. 2005.

[46] M. J. Silva and L. J. Gibson. "The effects of non-periodic microstructure and defects on the compressive strength of two-dimensional cellular solids." **International Journal of Mechanical Science**, vol. 39, no. 5, pp. 549-563, 1997.

[47] H. Sun , G. S. Sur and J. E. Mark. "Microcellular foams from poly-ethersulfone and poly-phenylsulfone preparation and mechanical properties." **European Polymer Journal**, vol. 38, pp. 2373-2381, 2002.

[48] R. E. Murray, J. E. Weller, V. Kumar. "Solid-state microcellular acrylonitrile-butadiene-styrene foams", **Cellular Polymers**, vol. 19, no. 6, pp. 413-425, 2000.

[49] V. Kumar and J. E. Weller. "A process to produce microcellular PVC", **International Polymer Processing VIII**, vol. 1, pp. 73-80 , 1993.

[50] V. Kumar and J. E. Weller. "Production of microcellular polycarbonate using carbon dioxide for bubble nucleation.", **Journal of Engineering for Industry**. vol. 116, pp. 413-420, 2004.

[51] Srichay P. and Methakul P. **"Microcellular bio-gradable plastic foam from tapioca starch."** Special Project Dissertation, Department of Chemical Engineering, King Mongkut's Institute of Technology Ladkrabang. 2005.

[52] P. Spitael and C. W. Macosko. "Strain hardening in polypropylenes and its role in extrusion foaming." **Polymer Engineering and Science**, vol. 44, no. 11, pp. 2091-2100, 2004.

[53] N. Chand, S. Sood, D. K. Singh and P. K. Rohatgi. "Structural and thermal studies on sisal fibre." **Journal of Thermal Analysis**, vol. 32, pp. 595-599, 1987.

[54] J. J. Schemenauer, T. A. Osswald, R. Sanadi and D. F. Caulfield. "Melt rheological properties of natural fiber-reinforced polypropylene." **ANTEC 2000 Society of Plastic Engineers Conference**, pp. 2206-2210, 2008.

[55] S. Li, P. K. Jarvela and P. A. Jarvela. "Melt rheological properties of polypropylene-maleated polypropylene blends – II. Dynamic viscoelastic properties." **Journal of Applied Polymer Science**, vol. 71, pp. 641-1648, 1999.

Appendices

Appendix A

Experimental Data from Recently Studies and Calculations of Surface Cell Density and Material Balance-Based Cell Density

Low density microcellular foams:

- Polyethersulfone foams, H. Sun *et al.* (2000) [50]
- Polyphenylsulfone foams, H. Sun *et al.* (2000) [50]

High density microcellular foams:

- Acrylonitrile-butadiene-styrene foams, E. Murray *et al.* (2000) [51]
- Polyvinylchloride foams, V. Kumar and J. Weller (1993) [52]
- Polycarbonate foams, V. Kumar and J. Weller (1994) [53]

Low density conventional foams:

- Polystyrene foams, P. Srichay and P. Methakul (2005) [54]

High density conventional foams:

- Polypropylene foams), P. Spitael and C. W. Macosko (2004) [55]

Table A.1 Surface cell density and material balance-based cell densities of PESF foams from a study by H. Sun *et al.* (2000).

Sample	Foaming temperature* (°C)	Density of polymer* (g/cm^3)	Relative density* (-)	Bubble Size* (μm)	Nucleus Density* (cell/cm3)	Expansion ratio (-)	Surface cell density ($cell/cm^2$)	Material balanced based cell density ($cell/cm^3$)
A01	120	1.37	0.86	2.0	2.92E+10	1.16	8.59E+06	3.34E+10
A02	140	1.37	0.76	2.8	7.60E+10	1.32	1.49E+07	2.09E+10
A03	160	1.37	0.68	4.2	5.20E+10	1.47	1.08E+07	8.25E+09
A04	175	1.37	0.60	6.3	3.20E+10	1.67	7.16E+06	3.06E+09
A05	184	1.37	0.55	8.5	2.73E+10	1.82	6.08E+06	1.40E+09
A06	190	1.37	0.44	-	-	2.27	-	-
A07	200	1.37	0.35	12.0	-	2.86	-	-
A08	210	1.37	0.33	-	-	3.03	-	-
A09	225	1.37	0.37	-	-	2.70	-	-

* Source: H. Sun *et al.* (2000) [47].

Table A.2 Surface cell density and material balance-based cell density of PPSF foams from a study by H. Sun *et al.* (2000).

Sample	Foaming temperature* (°C)	Density of polymer* (g/cm^3)	Relative density* (-)	Bubble Size* (μm)	Nucleus density* (cell/cm3)	Expansion ratio (-)	Surface cell density ($cell/cm^2$)	Material balanced based cell density ($cell/cm^3$)
B01	120	1.29	0.88	-	-	1.14	-	-
B02	140	1.29	0.78	1.3	2.45E+11	1.28	3.32E+07	1.91E+11
B03	160	1.29	0.69	2.4	2.35E+11	1.45	2.97E+07	4.28E+10
B04	175	1.29	0.63	3.3	1.38E+11	1.59	1.96E+07	1.97E+10
B05	184	1.29	0.57	4.2	2.15E+11	1.75	2.47E+07	1.11E+10

* Source: H. Sun *et al.* (2000) [47].

Table A.3 Surface cell density and material balance-based cell density of ABS foams from a study by E. Murray *et al.* (2000).

Sample	Saturation pressure* (MPa)	Foaming temperature* (°C)	Density of polymer* (g/cm^3)	Relative density* (g/cm^3)	Bubble Size* (μm)	Nucleus density* ($cell/cm^3$)	Expansion ratio (-)	Surface cell density ($cell/cm^2$)	Material balanced based cell density ($cell/cm^3$)
C01	0.350	105.0	1.04	0.88	0.90	2.7E+11	1.14	3.83E+07	3.14E+11
C02	0.350	110.0	1.04	0.66	1.06	2.2E+11	1.52	2.76E+07	5.45E+11
C03	0.350	115.0	1.04	0.45	1.50	1.8E+11	2.22	1.87E+07	3.11E+11
C04	1.0	90.0	1.04	0.86	0.61	9.8E+11	1.16	8.94E+07	1.18E+12
C05	1.0	100.0	1.04	0.51	1.13	8.2E+11	1.96	5.59E+07	6.49E+11
C06	2.0	70.0	1.04	0.97	0.54	4.7E+11	1.03	5.93E+07	3.64E+11
C07	2.0	80.0	1.04	0.71	1.03	3.6E+11	1.41	4.02E+07	5.07E+11
C08	2.0	90.0	1.04	0.49	1.29	2.3E+11	2.04	2.33E+07	4.54E+11
C09	3.0	60.3	1.04	0.90	0.83	4.0E+10	1.11	1.09E+07	3.34E+11
C10	3.0	70.2	1.04	0.70	0.90	5.3E+11	1.43	5.16E+07	7.86E+11
C11	3.0	80.0	1.04	0.53	1.32	1.1E+11	1.89	1.50E+07	3.90E+11
C12	3.0	90.0	1.04	0.36	2.58	6.8E+10	2.78	8.43E+06	7.12E+10
C13	4.0	60.0	1.04	0.77	0.22	1.8E+13	1.30	5.77E+08	4.13E+13
C14	4.0	80.0	1.04	0.45	1.81	8.8E+10	2.22	1.16E+07	1.77E+11
C15	4.0	100.0	1.04	0.17	2.08	5.9E+10	5.88	4.65E+06	1.76E+11
C16	5.0	80.0	1.04	0.38	0.27	1.4E+13	2.63	3.05E+08	6.02E+13
C17	5.0	100.0	1.04	0.28	0.48	1.4E+12	3.57	5.36E+07	1.24E+13

* Source: E. Murray *et al.* (2000) [48].

Table A.4 Surface cell density and material balance-based cell density of PVC foams from a study by V. Kumar and J. Weller (1993).

Sample	Saturated pressure* (MPa)	Foaming temperature* (°C)	Foaming time* (s)	Density of polymer* (g/cm^3)	Density of foam* (g/cm^3)	Bubble size* (μm)	Nucleus density* ($cell/cm^3$)	Expansion ratio (-)	Surface cell density ($cell/cm^2$)	Material balanced based cell density ($cell/cm^3$)
D01	4.8	56.0	30	1.33	1.22	9.22	0.20E+08	1.09	6.96E+04	2.02E+08
D02	4.8	60.6	30	1.33	1.03	10.29	0.84E+08	1.29	1.62E+05	3.95E+08
D03	4.8	65.2	30	1.33	0.96	9.38	2.48E+08	1.39	3.17E+05	6.44E+08
D04	4.8	70.1	30	1.33	0.79	10.00	2.70E+08	1.68	2.96E+05	7.75E+08
D05	4.8	75.1	30	1.33	0.63	9.21	6.99E+08	2.11	4.79E+05	1.29E+09
D06	4.8	80.2	30	1.33	0.53	9.90	7.95E+08	2.51	4.65E+05	1.18E+09
D07	4.8	84.8	30	1.33	0.47	10.13	9.56E+08	2.83	4.85E+05	1.19E+09
D08	4.8	89.9	30	1.33	0.32	8.36	18.1E+08	4.16	5.74E+05	2.48E+09
D09	4.8	95.0	30	1.33	0.32	8.63	55.9E+08	4.16	1.22E+06	2.26E+09
D10	4.8	100.0	30	1.33	0.29	8.46	41.3E+08	4.59	9.32E+05	2.47E+09
D11	4.8	105.0	30	1.33	0.21	13.16	10.3E+08	6.33	2.98E+05	7.06E+08
D12	4.8	110.0	30	1.33	0.25	10.12	7.99E+08	5.32	2.83E+05	1.50E+09
D13	4.8	115.0	30	1.33	0.25	10.50	14.3E+08	5.32	4.17E+05	1.34E+09
D14	4.8	120.0	30	1.33	0.40	7.36	28.0E+08	3.33	8.91E+05	3.35E+09

* Source: V. Kumar and J. Weller (1993) [49].

Table A.5 Surface cell density and material balance-based cell density of polycarbonate foams from a study by V. Kumar and J. Weller (1994).

Sample	Saturated pressure* (MPa)	Foaming temperature* (°C)	Foaming time* (s)	Density of polymer* (g/cm^3)	Density of foam* (g/cm^3)	Bubble size* (μm)	Nucleus density* ($cell/cm^3$)	Expansion ratio (-)	Surface cell density ($cell/cm^2$)	Material balanced based cell density ($cell/cm^3$)
E01	2.1	150	10	1.20	0.76	11.03	0.19E+09	1.58	2.44E+05	5.22E+08
E02	2.1	150	10	1.20	0.77	0.53	0.28E+09	1.56	3.18E+05	4.60E+12
E03	2.8	150	10	1.20	0.55	8.75	1.1E+09	2.18	6.34E+05	1.54E+09
E04	2.8	150	10	1.20	0.50	8.51	1.5E+09	2.40	7.31E+05	1.81E+09
E05	3.4	150	10	1.20	0.50	6.85	1.8E+09	2.40	8.25E+05	3.47E+09
E06	3.4	150	10	1.20	0.50	8.86	2.1E+09	2.40	9.15E+05	1.60E+09
E07	3.4	150	10	1.20	0.55	7.82	1.9E+09	2.18	9.12E+05	2.16E+09
E08	4.8	150	10	1.20	0.47	5.08	9.5E+09	2.55	2.40E+06	8.86E+09
E09	6.5	150	10	1.20	0.46	3.45	28.9E+09	2.61	4.97E+06	2.87E+10
E10	6.5	150	10	1.20	0.48	3.30	25.6E+09	2.50	4.72E+06	3.19E+10
E11	0.48	60.0	30	1.20	1.19	1.81	0.36E+09	1.01	5.03E+05	2.68E+09
E12	0.48	70.0	30	1.20	1.08	2.31	0.91E+09	1.11	8.76E+05	1.55E+10
E13	0.48	80.0	30	1.20	1.02	4.34	1.7E+09	1.18	1.28E+06	3.50E+09
E14	0.48	90.0	30	1.20	0.92	3.45	5.6E+09	1.30	2.65E+06	1.09E+10
E15	0.48	100.0	30	1.20	0.84	3.56	2.3E+09	1.43	1.37E+06	1.27E+10

* Source: V. Kumar and J. Weller (1994) [50].

Table A.5 Surface cell density and material balance-based cell density of polycarbonate foams from a study by V. Kumar and J. Weller (1994) (cont.).

Sample	Saturated pressure* (MPa)	Foaming temperature* (°C)	Foaming time* (s)	Density of polymer* (g/cm^3)	Density of foam* (g/cm^3)	Bubble size* (μm)	Nucleus density* ($cell/cm^3$)	Expansion ratio (-)	Surface cell density ($cell/cm^2$)	Material balanced based cell density ($cell/cm^3$)
E16	0.48	110.0	30	1.20	0.75	4.23	4.1E+09	1.60	1.87E+06	9.46E+09
E17	0.48	120.0	30	1.20	0.66	7.11	4.1E+09	1.82	1.72E+06	2.39E+09
E18	0.48	130.0	30	1.20	0.53	6.05	3.0E+09	2.26	1.21E+06	4.82E+09
E19	0.48	140.0	30	1.20	0.37	5.08	3.7E+09	3.24	1.09E+06	1.01E+10
E20	0.48	150.0	30	1.20	0.25	8.14	1.3E+09	4.80	4.19E+05	2.80E+09
E21	0.48	160.0	30	1.20	0.11	8.21	0.26E+09	10.91	8.28E+04	3.13E+09
E22	0.48	150	5.0	1.20	0.72	5.12	4.3E+09	1.67	1.88E+06	5.69E+09
E23	0.48	150	10.0	1.20	0.49	6.15	3.2E+09	2.45	1.19E+06	4.86E+09
E24	0.48	150	20.0	1.20	0.32	6.97	2.3E+09	3.75	7.22E+05	4.14E+09
E25	0.48	150	30.0	1.20	0.25	8.14	1.3E+09	4.80	4.19E+05	2.80E+09
E26	0.48	150	40.0	1.20	0.22	9.86	1.6E+09	5.45	4.42E+05	1.63E+09
E27	0.48	150	60.0	1.20	0.17	8.66	2.5E+09	7.06	5.01E+05	2.52E+09
E28	0.48	150	90.0	1.20	0.15	10.32	1.8E+09	8.00	3.70E+05	1.52E+09
E29	0.48	150	120.0	1.20	0.15	13.13	0.71E+09	8.00	1.99E+05	7.38E+08
E30	0.48	150	240.0	1.20	0.18	9.71	0.95E+09	6.67	2.73E+05	1.77E+09

* Source: V. Kumar and J. Weller (1994) [50].

Table A.6 Surface cell density and material balance-based cell density of polystyrene foams from a study by P. Srichay and P. Methakul (2005).

Sample	St-Bu-g-starch* (wt%)	PS* (wt%)	DEG* (phr)	Saturated pressure* (MPa)	Foaming temperature* (°C)	Bubble size* (μm)	Nucleus density* (cell/cm^3)	Expansion ratio* (-)	Surface cell density (cell/cm^2)	Material balanced based cell density (cell/cm^3)
F01	0	100	0	24.8	100	13.56	1.80E+08	2.030	1.99E+05	3.89E+08
F02	10	90	0	24.8	100	10.24	2.00E+09	2.063	9.80E+05	9.17E+08
F03	20	80	0	24.8	100	10.59	3.30E+09	1.922	1.43E+06	7.71E+08
F04	30	70	0	24.8	100	12.93	2.50E+09	1.829	1.23E+06	4.00E+08
F05	10	90	3	15.2	100	56.40	7.50E+07	2.380	9.98E+04	6.17E+06
F06	10	90	4	15.2	100	72.03	3.50E+08	2.399	2.77E+05	2.98E+06
F07	10	90	5	15.2	100	61.67	3.80E+07	2.628	5.94E+04	5.04E+06
F08	10	90	3	20.7	100	11.50	7.00E+09	2.733	1.87E+06	7.96E+08
F09	10	90	4	20.7	100	9.40	3.30E+09	3.563	9.50E+05	1.65E+09
F10	10	90	5	20.7	100	25.82	2.90E+09	3.819	8.32E+05	8.19E+07
F11	10	90	3	24.8	100	7.06	3.20E+09	1.861	1.44E+06	2.52E+09
F12	10	90	4	24.8	100	9.82	2.50E+09	2.014	1.16E+06	1.02E+09
F13	10	90	5	24.8	100	7.76	4.00E+09	2.129	1.52E+06	2.17E+09

* Source: P. Srichay and P. Methakul (2005) [51].

Table A.7 Surface cell density and material balance-based cell density of polypropylene foams from a study by P. Spitael and C. W. Macosko (2004).

Sample	PP1* (wt%)	PP2* (wt%)	PP2* (wt%)	CO_2* (wt%)	Density of polymer* (g/cm3)	Density of foam* (g/cm3)	Bubble size* (μm)	Nucleus density* (cell/cm3)	Expansion ratio (-)	Surface cell density (cell/cm^2)	Material balanced based cell density (cell/cm^3)
G01	100	0	0	4.2	0.92	0.26	61	7.4E+06	3.54	1.63E+04	6.04E+06
G02	100	0	0	5.2	0.92	0.12	63	21.2E+06	7.67	1.97E+04	6.64E+06
G03	75	25	0	4.2	0.92	-	-	-	-	-	-
G04	75	25	0	5.2	0.92	0.13	37	54.4E+06	7.08	3.89E+04	3.24E+07
G05	50	50	0	4.2	0.92	0.24	56	11.7E+06	3.83	2.11E+04	8.04E+06
G06	50	50	0	5.2	0.92	0.13	62	21.2E+06	7.08	2.08E+04	6.88E+06
G07	0	100	0	4.2	0.92	0.30	81	5.5E+06	3.07	1.48E+04	2.42E+06
G08	0	100	0	5.2	0.92	0.28	57	11.5E+06	3.29	2.30E+04	7.17E+06
G09	75	0	25	4.2	0.92	-	-	-	-	-	-
G10	75	0	25	5.2	0.92	0.21	62	10.7E+06	4.38	1.81E+04	6.18E+06
G11	50	0	50	4.2	0.92	0.12	89	14.6E+06	7.67	1.54E+04	2.36E+06
G12	50	0	50	5.2	0.92	0.05	66	30.2E+06	18.40	1.39E+04	6.28E+06

* Source: P. Spitael and C. W. Macosko (2004) [52].

Appendix B

Percentage Average Absolute Deviation of Conventional, FCC-PF, and FCC-NPF models

Table B.1 Percentages average absolute deviations of conventional, FCC-PF, and FCC-NPF models of microcellular low density foams.

Sample	Material balanced based cell density ($cell/cm^3$)	Conventional cell density ($cell/cm^3$)	%AAD	FCC-PF cell density ($cell/cm^3$)	%AAD	FCC-NPF cell density ($cell/cm^3$)	%AAD
A01	3.34E+10	2.52E+10	24.63	2.87E+10	14.10	3.66E+09	89.05
A02	2.09E+10	5.76E+10	175.48	6.56E+10	213.99	8.37E+09	59.97
A03	8.25E+09	3.54E+10	328.78	4.03E+10	388.72	5.14E+09	37.70
A04	3.06E+09	1.92E+10	526.20	2.18E+10	613.74	2.78E+09	9.01
A05	1.40E+09	1.50E+10	971.43	1.71E+10	1121.21	2.18E+09	55.68
A06	-	-	-	-	-	-	-
A07	-	-	-	-	-	-	-
A08	-	-	-	-	-	-	-
A09	-	-	-	-	-	-	-
B01	-	-	-	-	-	-	-
B02	1.91E+11	1.91E+11	0.21	2.18E+11	14.22	2.78E+10	85.44
B03	4.28E+10	1.62E+11	278.67	1.85E+11	331.60	2.35E+10	44.98
B04	1.97E+10	8.68E+10	340.57	9.89E+10	402.16	1.26E+10	35.99
B05	1.11E+10	1.23E+11	1006.82	1.40E+11	1161.5	1.79E+10	60.82
		Average	405.87	Average	473.48	Average	53.18

Table B.2 Percentages average absolute deviations of conventional, FCC-PF, and FCC-NPF models of microcellular high density foams.

Sample	Material balanced based cell density (cell/cm^3)	Conventional cell density (cell/cm^3)	%AAD	FCC-PF cell density (cell/cm^3)	%AAD	FCC-NPF cell density (cell/cm^3)	%AAD
C01	3.14E+11	2.37E+11	24.57	2.70E+11	14.03	3.44E+10	89.04
C02	5.45E+11	1.45E+11	73.44	1.65E+11	69.73	2.10E+10	96.14
C03	3.11E+11	8.11E+10	73.93	9.24E+10	70.28	1.18E+10	96.21
C04	1.18E+12	8.45E+11	28.40	9.63E+11	18.40	1.23E+11	89.60
C05	6.49E+11	4.18E+11	35.54	4.77E+11	26.52	6.08E+10	90.63
C06	3.64E+11	4.56E+11	25.36	5.20E+11	42.89	6.63E+10	81.79
C07	5.07E+11	2.55E+11	49.64	2.91E+11	42.60	3.71E+10	92.68
C08	4.54E+11	1.13E+11	75.17	1.29E+11	71.69	1.64E+10	96.39
C09	3.34E+11	3.60E+10	89.21	4.11E+10	87.70	5.24E+09	98.43
C10	7.86E+11	3.71E+11	52.85	4.22E+11	46.25	5.39E+10	93.15
C11	3.90E+11	5.82E+10	85.08	6.63E+10	82.99	8.46E+09	97.83
C12	7.12E+10	2.45E+10	65.65	2.79E+10	60.84	3.55E+09	95.01
C13	4.13E+13	1.38E+13	66.47	1.58E+13	61.79	2.01E+12	95.13
C14	1.77E+11	3.96E+10	77.60	4.52E+10	74.47	5.76E+09	96.75
C15	1.76E+11	1.00E+10	94.30	1.14E+10	93.50	1.46E+09	99.17
C16	6.02E+13	5.32E+12	91.16	6.07E+12	89.92	7.73E+11	98.72
C17	1.24E+13	3.92E+11	96.84	4.47E+11	96.40	5.70E+10	99.54
D01	2.02E+08	1.83E+07	90.92	2.09E+07	89.65	2.67E+06	98.68
D02	3.95E+08	6.51E+07	83.51	7.42E+07	81.21	9.46E+06	97.60
D03	6.44E+08	1.78E+08	72.30	2.03E+08	68.42	2.59E+07	95.97
D04	7.75E+08	1.61E+08	79.26	1.83E+08	76.36	2.34E+07	96.99
D05	1.29E+09	3.31E+08	74.32	3.78E+08	70.73	4.81E+07	96.27
D06	1.18E+09	3.17E+08	73.16	3.61E+08	69.41	4.60E+07	96.10
D07	1.19E+09	3.38E+08	71.61	3.85E+08	67.64	4.91E+07	95.88
D08	2.48E+09	4.35E+08	82.46	4.96E+08	80.00	6.32E+07	97.45
D09	2.26E+09	1.34E+09	40.54	1.53E+09	32.23	1.95E+08	91.36
D10	2.47E+09	9.00E+08	63.57	1.03E+09	58.48	1.31E+08	94.71
D11	7.06E+08	1.63E+08	76.95	1.85E+08	73.73	2.36E+07	96.65
D12	1.50E+09	1.50E+08	89.99	1.71E+08	88.59	2.18E+07	98.55
D13	1.34E+09	2.69E+08	79.94	3.06E+08	77.14	3.91E+07	97.09
D14	3.35E+09	8.41E+08	74.90	9.58E+08	71.39	1.22E+08	96.35

Table B.2 Percentages average absolute deviations of conventional, FCC-PF, and FCC-NPF models of microcellular high density foams. (cont.)

Sample	Material balanced based cell density ($cell/cm^3$)	Conventional cell density ($cell/cm^3$)	%AAD	FCC-PF cell density ($cell/cm^3$)	%AAD	FCC-NPF cell density ($cell/cm^3$)	%AAD
E01	5.22E+08	1.20E+08	76.96	1.37E+08	73.74	1.75E+07	96.65
E02	4.60E+12	1.79E+08	100.00	2.05E+08	100.00	2.61E+07	100.00
E03	1.54E+09	5.05E+08	67.23	5.75E+08	62.65	7.33E+07	95.24
E04	1.81E+09	6.25E+08	65.47	7.12E+08	60.64	9.08E+07	94.98
E05	3.47E+09	7.50E+08	78.39	8.55E+08	75.36	1.09E+08	96.86
E06	1.60E+09	8.75E+08	45.31	9.97E+08	37.67	1.27E+08	92.05
E07	2.16E+09	8.72E+08	59.65	9.93E+08	54.01	1.27E+08	94.14
E08	8.86E+09	3.73E+09	57.95	4.25E+09	52.07	5.41E+08	93.89
E09	2.87E+10	1.11E+10	61.42	1.26E+10	56.03	1.61E+09	94.39
E10	3.19E+10	1.02E+10	67.90	1.17E+10	63.41	1.49E+09	95.34
E11	2.68E+09	3.56E+08	86.70	4.06E+08	84.84	5.18E+07	98.07
E12	1.55E+10	8.20E+08	94.71	9.34E+08	93.97	1.19E+08	99.23
E13	3.50E+09	1.44E+09	58.84	1.64E+09	53.08	2.09E+08	94.02
E14	1.09E+10	4.31E+09	60.48	4.91E+09	54.95	6.26E+08	94.26
E15	1.27E+10	1.61E+09	87.34	1.83E+09	85.57	2.34E+08	98.16
E16	9.46E+09	2.56E+09	72.91	2.92E+09	69.13	3.72E+08	96.06
E17	2.39E+09	2.25E+09	5.74	2.57E+09	7.43	3.27E+08	86.30
E18	4.82E+09	1.33E+09	72.46	1.51E+09	68.61	1.93E+08	96.00
E19	1.01E+10	1.14E+09	88.69	1.30E+09	87.11	1.66E+08	98.36
E20	2.80E+09	2.71E+08	90.33	3.09E+08	88.98	3.94E+07	98.59
E21	3.13E+09	2.38E+07	99.24	2.72E+07	99.13	3.46E+06	99.89
E22	5.69E+09	2.57E+09	54.75	2.93E+09	48.42	3.74E+08	93.42
E23	4.86E+09	1.31E+09	73.13	1.49E+09	69.37	1.90E+08	96.10
E24	4.14E+09	6.13E+08	85.19	6.99E+08	83.11	8.91E+07	97.85
E25	2.80E+09	2.71E+08	90.33	3.09E+08	88.98	3.94E+07	98.59
E26	1.63E+09	2.94E+08	81.99	3.35E+08	79.47	4.27E+07	97.38
E27	2.52E+09	3.54E+08	85.95	4.04E+08	83.98	5.15E+07	97.96
E28	1.52E+09	2.25E+08	85.20	2.56E+08	83.13	3.27E+07	97.85
E29	7.38E+08	8.88E+07	87.97	1.01E+08	86.29	1.29E+07	98.25
E30	1.77E+09	1.42E+08	91.95	1.62E+08	90.83	2.07E+07	98.83
		Average	72.01	Average	68.80	Average	95.81

Table B.3 Percentages average absolute deviations of conventional, FCC-PF, and FCC-NPF models of conventional low density foams.

Sample	Material balanced based cell density ($cell/cm^3$)	Conventional cell density ($cell/cm^3$)	%AAD	FCC-PF cell density ($cell/cm^3$)	%AAD	FCC-NPF cell density ($cell/cm^3$)	%AAD
F01	3.89E+08	8.87E+07	77.21	1.01E+08	74.02	1.29E+07	96.69
F02	9.17E+08	9.69E+08	5.72	1.10E+09	20.50	1.41E+08	84.64
F03	7.71E+08	1.72E+09	122.69	1.96E+09	153.83	2.49E+08	67.64
F04	4.00E+08	1.37E+09	241.72	1.56E+09	289.49	1.99E+08	50.35
F05	6.17E+06	3.15E+07	410.74	3.59E+07	482.14	4.58E+06	25.79
F06	2.98E+06	1.46E+08	4795.78	1.66E+08	5480.21	2.12E+07	611.36
F07	5.04E+06	1.45E+07	186.90	1.65E+07	227.01	2.10E+06	58.31
F08	7.96E+08	2.56E+09	221.77	2.92E+09	266.75	3.72E+08	53.25
F09	1.65E+09	9.26E+08	43.87	1.06E+09	36.02	1.35E+08	91.84
F10	8.19E+07	7.59E+08	827.18	8.66E+08	956.80	1.10E+08	34.72
F11	2.52E+09	1.72E+09	31.77	1.96E+09	22.23	2.50E+08	90.09
F12	1.02E+09	1.24E+09	21.70	1.41E+09	38.71	1.80E+08	82.32
F13	2.17E+09	1.88E+09	13.42	2.14E+09	1.31	2.73E+08	87.42
		Average	538.50	Average	619.15	Average	110.34

Table B.4 Percentages average absolute deviations of conventional, FCC-PF and FCC-NPF models of conventional high density foams.

Sample	Material balanced based cell density ($cell/cm^3$)	Conventional cell density ($cell/cm^3$)	%AAD	FCC-PF cell density ($cell/cm^3$)	%AAD	FCC-NPF cell density ($cell/cm^3$)	%AAD
G01	6.04E+06	2.09E+06	65.39	2.38E+06	60.55	3.04E+05	94.97
G02	6.64E+06	2.76E+06	58.37	3.15E+06	52.55	4.02E+05	93.95
G03	-	-	-	-	-	-	-
G04	3.24E+07	7.68E+06	76.29	8.76E+06	72.97	1.12E+06	96.55
G05	8.04E+06	3.05E+06	62.00	3.48E+06	56.69	4.44E+05	94.48
G06	6.88E+06	2.99E+06	56.48	3.41E+06	50.39	4.35E+05	93.68
G07	2.42E+06	1.79E+06	25.97	2.04E+06	15.62	2.60E+05	89.24
G08	7.17E+06	3.50E+06	51.25	3.98E+06	44.43	5.08E+05	92.92
G09	-	-	-	-	-	-	-
G10	6.18E+06	2.44E+06	60.47	2.78E+06	54.94	3.55E+05	94.26
G11	2.36E+06	1.90E+06	19.34	2.17E+06	8.07	2.77E+05	88.28
G12	6.28E+06	1.64E+06	73.86	1.87E+06	70.21	2.38E+05	96.20
		Average	54.94	Average	48.64	Average	93.45

Appendix C

Experimental Data

Table C.1 Experimental data of polyethylene foams

Sample	Polymer A (wt%)	Polymer B (wt%)	Nucleating agent (phr)	Cell size (μm)	Density of polymer (g/cm^3)	Density of foam (g/cm^3)	Expansion ratio (-)	Surface cell density ($cell/cm^2$)	Material balance based cell density (cell/cm3)	Standard cell density; LD (cell/cm3)	Isotropic foam index (-)
X01	85	15	0	23.8	0.948	0.256	3.70	1.78E+05	1.03E+08	1.09E+07	0.98
X02	85	15	0.4	56.1	0.944	0.124	7.61	6.08E+04	9.43E+06	2.18E+06	0.64
X03	85	15	1	37.0	0.936	0.200	4.68	1.39E+05	2.96E+07	7.55E+06	0.59
X04	80	20	0	32.6	0.946	0.298	3.17	1.13E+05	3.77E+07	5.52E+06	0.83
X05	80	20	0.4	37.3	0.943	0.210	4.49	1.37E+05	2.86E+07	7.39E+06	0.59
X06	80	20	1	45.5	0.936	0.351	2.67	9.24E+04	1.27E+07	4.08E+06	0.49

Table C.2 Experimental data of sisal fiber/polypropylene composite foams

Sample	PP (wt%)	MA-g-PP (wt%)	Sisal fiber (phr)	Cell size (μm)	Density of polymer (g/cm^3)	Density of foam (g/cm^3)	Expansion ratio (-)	Surface cell density ($cell/cm^2$)	Material balance based cell density (cell/cm3)	Standard cell density; LD (cell/cm3)	Isotropic foam index (-)
Y01	100	0	0	4.3	0.904	0.196	4.52	7.17E+06	1.87E+10	2.79E+09	0.83
Y02	100	0	20	6.2	0.955	0.813	1.17	9.57E+05	1.16E+09	1.36E+08	0.93
Y03	98	2	20	17.1	0.934	0.541	1.73	3.22E+05	1.61E+08	2.65E+07	0.78
Y04	95	5	20	18.5	0.929	0.580	1.60	4.31E+05	1.13E+08	4.11E+07	0.44
Y05	90	10	20	28.5	0.947	0.578	1.64	1.19E+05	3.22E+07	5.96E+06	0.73

Author Biography

Piyapong Buahom was born on 30 January 1986 in Phoncharoen, Nongkhai, Thailand. In March 2008, he was received his degree in Bachelor of Engineering in Chemical Engineering at King Mongkut's Institute of Technology Ladkrabang, Bangkok, Thailand. He had successfully completed a training period with the Process Engineering Department, as a student trainee in WorleyParsons (Thailand) co. ltd. from April to May 2007.

During these two years for Master of Engineering program in Chemical Engineering at KMITL, his work at Polymer Processing and Supercritical Fluid Technology Research Group involved characterization of polymeric foams, polymeric foam processing, and supercritical fluid technology.

Publications:

1. **P. Buahom** and S. Areerat. "Characterization of foam cell density with principle of critical bubble lattice." **Proceeding of Polymer Processing Society 26th Annual Meeting, PPS-26,** Banff, Canada, G10-640, 2010.
2. **P. Buahom** and S. Areerat. "Characterization of cell density for isotropic closed-cell polymeric foams with analysis of critical bubble packed structure." **Ladkrabang Engineering Journal**, vol. 27, no. 1, pp. 49-54, 2010.
3. P. Maskong, **P. Buahom**, P. Piyamanocha, W. Rungseesantivanon and S. Areerat. "Effect of fiber surface treatment on mechanical properties of jute reinforced PU composite foams." **Proceeding of Japan Society of Polymer Processing Annual Meeting, JSPP 2008**, Tokyo, Japan, 2008.